



POLITECNICO DI TORINO

I Facoltà di Ingegneria

DIPARTIMENTO DI INGEGNERIA MECCANICA E
AEROSPAZIALE

Thesis / PFC

**GLOBAL LOCAL ANALYSIS OF COMPOSITE
AIRCRAFT STRUCTURES**

Tutors:

Prof. Erasmo Carrera, Prof. Alfonso Pagani, Dott. Alberto García

Student:

Artur Margarit Sol

March 2019

Contents

Summary	3
1 Fundamentals of beam and plate structures	5
1.1 Preliminars	5
1.2 Fundamentals of elasticity	6
1.2.1 Stress and Deformation vectors	6
1.2.2 Linear Strain-Displacement relations	8
1.2.3 Hooke's law	10
1.3 Beam theories	11
1.3.1 Euler-Bernoulli Beam Theory	11
1.3.2 Timoshenko Beam Theory	13
1.4 Plate theories	15
1.4.1 Classical plate model Kirchoff-Love	15
1.4.2 Reissner and Mindlin plate model	16
2 Carrera Unified Formulation - CUF theory	17
2.1 Displacement field for one dimensional models	17
2.1.1 Taylor expansions	20
2.1.2 Lagrange Expansion	21
2.2 Displacement field for two dimensional models	23
2.3 Governing equation and stiffness matrix	24
2.4 Loading vector	28
3 Composite materials	30
3.1 Composite materials in aeronautics	31
3.2 Composite laminates	33

3.3	CUF formulation for composite laminates	33
3.3.1	Beam models	34
3.3.2	Plate models	36
4	Mul2 code	38
5	Global Local Analysis	44
5.1	Application of the boundary conditions	45
5.2	Global local process and Python interface	47
5.2.1	Beam interface	49
5.2.2	Plate interface	50
5.2.3	Element wise interface	50
5.2.4	The bdf file	51
6	Numerical results - Beam model	52
6.1	Cantilivered C section beam	52
6.2	Eight layer beam	54
6.2.1	Global model	54
6.2.2	Global local model	55
7	Numerical Results - Plate Model	58
7.1	3 Ply Composite Rectangular Plate Under Bending	58
7.2	Plate hole: the element wise approach	61
7.3	Wing structure	65
7.3.1	Local analysis around the hole	68
7.3.2	Element wise analysis	74
8	Conclusions	77
9	Apendix	79
9.1	Python plate interface manual	79
9.2	Element wise interface manual	82

Summary

In the field of the structural analysis, classical beam and plate theories are usually used although those theories have serious limitations. In the field of the aerospace, specially for composite laminates, this theories can lead to an errors (for example in free edge analysis, torsion or in-plane deformations).

The aim of this work is to present the Carrera Unified Formulation, a theory which overcome the limits of classical theories with a low computational cost (On contrast with the solid models that have a high computational costs). This formulation can be used to analyse a global model or to perform a local analysis in a complex region of a global model. In order to carry this last type of analysis a Python interface between the global model (designed with a commercial software) and the Mul2 code (software based on CUF designed by the Department of Mechanical and Aerospace engineering of Polito) has been developed during this thesis.

To summarize the structure and the content of this thesis, a brief explanation of each chapter is provided next.

Chapter 1 presents the fundamentals of elasticity and the classical beam and plates theories. Stress and deformations vectors, strain - displacements relations and the Hooke's law are explained in the fundamentals of elasticity. An approach on the Euler Bernoulli Beam theory (EBBT), Timoshenko Beam Theory (TBT), Kirchoff-Love classical plate theory and Reissner-Midlin plate theory is presented. The displacement field, the strain-displacements relations and constitutive equations of each model are explained in this chapter.

The Carrera Unified Formulation (CUF) is presented in **Chapter 2**. How it works for beam and plates, the displacements fields for each model and the Taylor and Lagrange expansions functions are explained in this chapter. An introduction to finite element formulation

as well as the construction of the governing equations, stiffness matrix and loading vector are also described.

In **Chapter 3** a brief introduction to composite materials laminates and composites aircraft is presented. The history about this type of materials and their use in the aerospace industry is summarized and the importance of composite laminates in this industry is explained.

Chapter 4 presents the Mul 2 code. This code is been developed by the Department of Mechanical and Aerospace Engineering of Politecnico di Torino by a research group lead by Erasmo Carrera. This software is based in CUF and works for beams, plates and shells in different fields and applications. In this chapter it is explained how is this software used during the thesis.

The global local approach is introduced in **Chapter 5**. The application of the boundary conditions between the global model and the local region is described and the python interface in charge of connect the global model designed by a commercial code with the Mul2 code (the software in charge of the local analysis) is presented. In the appendix a manuals of the plate Python interface and element wise Python interface can be found.

The numerical results for beam and plate examples are displayed in **Chapter 6** and **Chapter 7**. A comparison between the results with the global local approach and those provided by the commercial software Nastran are shown.

Finally the conclusions of this work are presented in **Chapter 8**.

Chapter 1

Fundamentals of beam and plate structures

1.1 Preliminars

For the next chapters the reference system adopted for the beam structures is Cartesian axes represented at Fig.1.1.

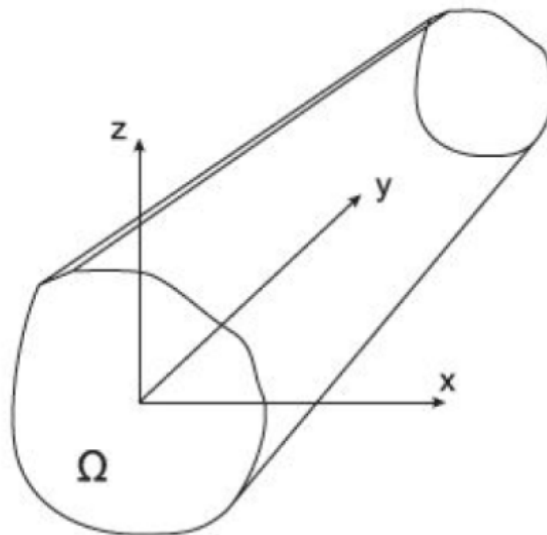


Figure 1.1: Beam reference system

The reference system above is referred to a beam whose axial extension (L) is clearly predominant in comparison with any other orthogonal dimension. x - z beam cross section is indicated with Ω .

The reference system used for plate structures is displayed in Fig.1.2, considering in this

case the dimension of the cross section predominant in comparison with the dimension along z axis (thickness direction).

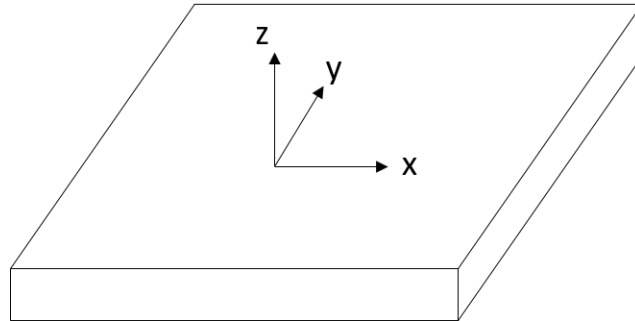


Figure 1.2: Plate reference system

The displacement field vector referring to the reference system of beam or plate is the following:

$$\mathbf{u}(x, y, z; t) = \left\{ \begin{array}{l} u(x, y, z) \\ v(x, y, z) \\ w(x, y, z) \end{array} \right\} \quad (1.1)$$

The terms u_x , u_y and u_z are the components along x, y and z respectively depending on the position where are evaluated. This variables are usually the solution of the problem and the theory of the elasticity focuses in the determination of these.

1.2 Fundamentals of elasticity

1.2.1 Stress and Deformation vectors

The stress and deformation vectors are introduced. In Fig.1.3 the stress and deformation components are represented.

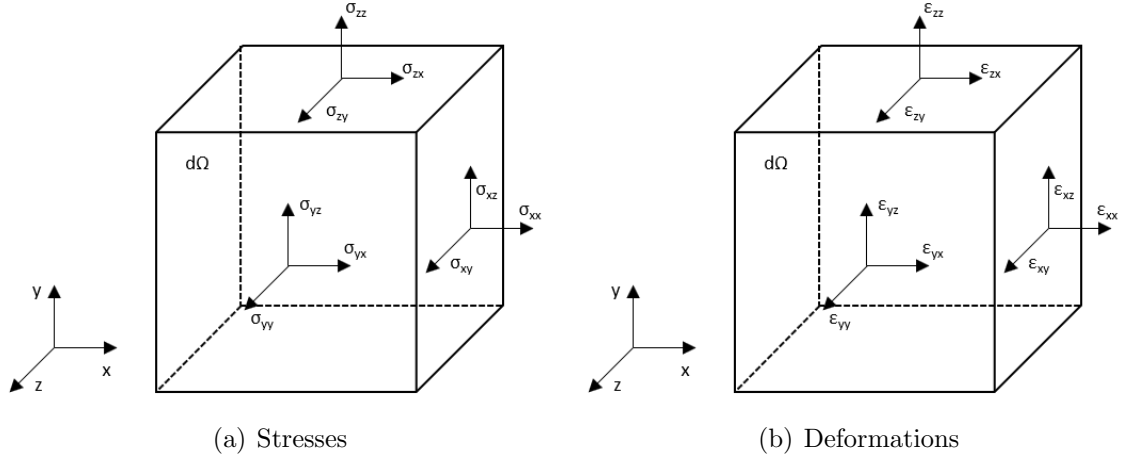


Figure 1.3: Stress and Deformation components

For each plane there are three stress components resulting in a total of 9 components. They can be write in a matrix where the normal components are placed at the diagonal. This matrix is called stress tensor:

$$\sigma = \begin{bmatrix} \sigma_{xx} & \sigma_{xy} & \sigma_{xz} \\ \sigma_{yx} & \sigma_{yy} & \sigma_{zx} \\ \sigma_{zx} & \sigma_{zy} & \sigma_{zz} \end{bmatrix} \quad (1.2)$$

This tensor has the particularity, following the Cauchy's theorem, that the shear stress are equal 2 to 2. This is $\sigma_{ij} = \sigma_{ji}$, resulting to a symmetric stress tensor with only six different components to define the stress state. This components can be written in a column vector like:

$$\sigma^T = \left\{ \sigma_{xx} \quad \sigma_{yy} \quad \sigma_{zz} \quad \sigma_{xy} \quad \sigma_{xz} \quad \sigma_{yz} \right\} \quad (1.3)$$

The deformation components can be also written in matrix form the same way as the stresses. The matrix is called strain tensor:

$$\varepsilon = \begin{bmatrix} \epsilon_{xx} & \epsilon_{xy} & \epsilon_{xz} \\ \epsilon_{yx} & \epsilon_{yy} & \epsilon_{zx} \\ \epsilon_{zx} & \epsilon_{zy} & \epsilon_{zz} \end{bmatrix} \quad (1.4)$$

The strain tensor is also symmetric being $\epsilon_{ij} = \epsilon_{ji}$, so it can be written as a column vector:

$$\epsilon^T = \left\{ \epsilon_{xx} \quad \epsilon_{yy} \quad \epsilon_{zz} \quad \epsilon_{xy} \quad \epsilon_{xz} \quad \epsilon_{yz} \right\} \quad (1.5)$$

Usually both stresses and strains are divided in two different groups regarding if they are orthogonal or tangent to the cross-section. So, the previous vectors can be rewrite as:

$$\begin{aligned}\boldsymbol{\sigma}_n &= \left\{ \begin{matrix} \sigma_{yy} & \sigma_{xy} & \sigma_{yz} \end{matrix} \right\}^T \\ \boldsymbol{\epsilon}_n &= \left\{ \begin{matrix} \varepsilon_{yy} & \varepsilon_{xy} & \varepsilon_{yz} \end{matrix} \right\}^T\end{aligned}\tag{1.6}$$

$$\begin{aligned}\boldsymbol{\sigma}_\Omega &= \left\{ \begin{matrix} \sigma_{xx} & \sigma_{zz} & \sigma_{xz} \end{matrix} \right\}^T \\ \boldsymbol{\epsilon}_\Omega &= \left\{ \begin{matrix} \varepsilon_{xx} & \varepsilon_{zz} & \varepsilon_{xz} \end{matrix} \right\}^T\end{aligned}\tag{1.7}$$

The sub-indexes n and ω refer to the normal and in-plan components of the vector respectively.

1.2.2 Linear Strain-Displacement relations

Assuming "small deformations" the strain components can be linear related with the displacement components as following:

$$\begin{aligned}\epsilon_{xx} &= \frac{\partial u}{\partial x} \\ \epsilon_{yy} &= \frac{\partial v}{\partial y} \\ \epsilon_{zz} &= \frac{\partial w}{\partial z} \\ \epsilon_{xy} &= \frac{1}{2} \left(\frac{\partial u}{\partial y} + \frac{\partial v}{\partial x} \right) \\ \epsilon_{zx} &= \frac{1}{2} \left(\frac{\partial w}{\partial x} + \frac{\partial u}{\partial z} \right) \\ \epsilon_{zy} &= \frac{1}{2} \left(\frac{\partial w}{\partial y} + \frac{\partial v}{\partial z} \right)\end{aligned}\tag{1.8}$$

Regrouping the strains again in the normal and in-plane components the previous equations can be written as:

$$\begin{aligned}\boldsymbol{\epsilon}_n^T &= \left\{ \begin{matrix} v_{,y} & v_{,z} + w_{,y} & v_{,x} + u_{,y} \end{matrix} \right\} \\ \boldsymbol{\epsilon}_\Omega^T &= \left\{ \begin{matrix} u_{,x} & w_{,x} & u_{,z} + w_{,x} \end{matrix} \right\}\end{aligned}\tag{1.9}$$

Where the comma indicates the derivation symbol and the coordinate after it the derivation direction.

To simplify the expression, the matrix notation is used. The previous equation are rewritten as:

$$\begin{aligned}\epsilon_{\Omega} &= D_{\Omega}u \\ \epsilon_n &= D_n u = (D_{n\Omega} + D_{nn})u\end{aligned}\tag{1.10}$$

where D_{Ω} , $D_{n\Omega}$ and D_{nn} are the differential matrix operators defined as:

$$\begin{aligned}D_{\Omega} &= \begin{bmatrix} 0 & 0 & \frac{\partial}{\partial z} \\ \frac{\partial}{\partial x} & 0 & 0 \\ \frac{\partial}{\partial z} & 0 & \frac{\partial}{\partial x} \end{bmatrix} \\ D_{n\Omega} &= \begin{bmatrix} 0 & \frac{\partial}{\partial z} & 0 \\ 0 & \frac{\partial}{\partial x} & 0 \\ 0 & 0 & 0 \end{bmatrix}\end{aligned}\tag{1.11}$$

$$D_{nn} = \begin{bmatrix} 0 & 0 & \frac{\partial}{\partial y} \\ \frac{\partial}{\partial y} & 0 & 0 \\ 0 & \frac{\partial}{\partial y} & 0 \end{bmatrix}$$

The geometrical relations between strains and displacements can also be defined with the compact vectorial notation as:

$$\epsilon = Du\tag{1.12}$$

where D in the compact form is the following linear differential operator:

$$D = \begin{bmatrix} 0 & \frac{\partial}{\partial y} & 0 \\ \frac{\partial}{\partial x} & 0 & 0 \\ 0 & 0 & \frac{\partial}{\partial z} \\ \frac{\partial}{\partial z} & 0 & \frac{\partial}{\partial x} \\ 0 & \frac{\partial}{\partial z} & \frac{\partial}{\partial y} \\ \frac{\partial}{\partial y} & \frac{\partial}{\partial x} & 0 \end{bmatrix}\tag{1.13}$$

1.2.3 Hooke's law

The Hooke's law define a relation between strain and stresses assuming a linear elastic behaviour of the material which suffers the deformation. This relation is defined as following:

$$\boldsymbol{\sigma} = \mathbf{C} \boldsymbol{\epsilon} \quad (1.14)$$

where \mathbf{C} is the stiffness matrix which relates both variables. Considering the previous notation, the Hooke's law can be defined like:

$$\begin{aligned} \sigma_n &= C_{nn}\epsilon_n + C_{n\Omega}\epsilon_\Omega \\ \sigma_\Omega &= C_{\Omega n}\epsilon_n + C_{\Omega\Omega}\epsilon_\Omega \end{aligned} \quad (1.15)$$

where the matrix \mathbf{C} has been divided in four different parts considering the normal or in-plane components of the stresses and strains.

In case the material is isotropic, the matrix \mathbf{C} can be written as following:

$$\mathbf{C} = \begin{bmatrix} C_{33} & C_{23} & C_{13} & 0 & 0 & 0 \\ C_{23} & C_{22} & C_{12} & 0 & 0 & 0 \\ C_{13} & C_{12} & C_{11} & 0 & 0 & 0 \\ 0 & 0 & 0 & C_{44} & 0 & 0 \\ 0 & 0 & 0 & 0 & C_{55} & 0 \\ 0 & 0 & 0 & 0 & 0 & C_{66} \end{bmatrix} \quad (1.16)$$

The coefficients of the stiffness matrix depend only on the Young's modulus, E , and the Poisson ratio, ν , and they are:

$$\begin{aligned} C_{11} &= C_{22} = C_{33} = \frac{(1-\nu)E}{(1+\nu)(1-2\nu)} \\ C_{12} &= C_{13} = C_{23} = \frac{\nu E}{(1+\nu)(1-2\nu)} \\ C_{44} &= C_{55} = C_{66} = \frac{E}{2(1+\nu)} \end{aligned} \quad (1.17)$$

1.3 Beam theories

1.3.1 Euler-Bernoulli Beam Theory

The Euler-Bernoulli beam theory, or EBBT, is a simplified model that is used for the case of a beam with only lateral loads and small deflections. This model relies in three assumptions: The **first** one is that the cross-sections remains always rigid, plane and normal to the deformed axis of the beam. This can be written as follows:

$$\begin{aligned}\epsilon_{xx} &= \frac{\partial u}{\partial x} = 0 \\ \epsilon_{zz} &= \frac{\partial w}{\partial z} = 0 \\ \epsilon_{zx} &= \frac{1}{2} \left(\frac{\partial w}{\partial x} + \frac{\partial u}{\partial z} \right) = 0\end{aligned}\tag{1.18}$$

The **second** assumption to be made is that the cross-section of the beam (this is the x-z plane) rotates around a neutral surface causing that the axial displacement is linear along the axis x and z. That can be write mathematically as:

$$v(x, y, z) = v_1 + \phi_z(y)x + \phi_x(y)z\tag{1.19}$$

The **third** and last assumption is that the cross-section remains perpendicular to the neutral surface when loads are applied. This cause that the shear strains ϵ_{xy} and ϵ_{yz} are approximate to 0. So,

$$\epsilon_{xy} = \epsilon_{yz} = 0\tag{1.20}$$

Considering this last assumption it can be derived that the rotations of the section around x and z are equal to the variation of the axial displacements along the axis z and x respectively as it can be observed in Fig.1.4,

$$\begin{aligned}\phi_z &= - \frac{\partial v}{\partial x} \\ \phi_x &= \frac{\partial v}{\partial z}\end{aligned}\tag{1.21}$$

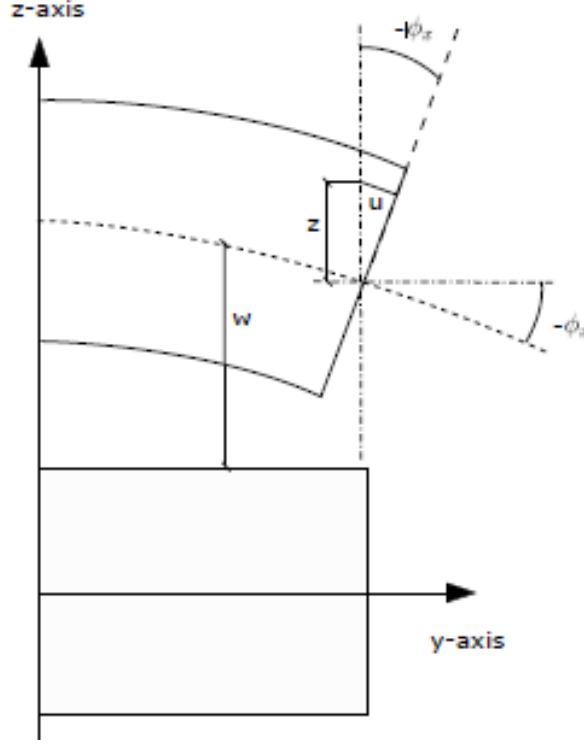


Figure 1.4: EBBT model of deformations

Considering Eq.1.20 and Eq.1.8 then the rotations along the z and x axis are:

$$\begin{aligned}\phi_z &= \frac{\partial u}{\partial y} \\ \phi_x &= -\frac{\partial w}{\partial y}\end{aligned}\tag{1.22}$$

With the three assumptions presented and considering a generic beam structure whose longitudinal axis lays on the coordinate y and its cross-section is defined in xz-plane. The kinematic field of EBBT can be write as:

$$\begin{aligned}u(x, y, z) &= u_1(y) \\ v(x, y, z) &= v_1(y) - x \frac{\partial u_1}{\partial y}(y) - z \frac{\partial w_1}{\partial y}(y) \\ w(x, y, z) &= w_1(y)\end{aligned}\tag{1.23}$$

where u_x , u_y and u_z are the components of the 3D displacement field vector along x, y and z respectively and u_{x_1} , u_{y_1} and u_{z_1} are the displacements of the beam axis. $\frac{\partial u_{x_1}}{\partial y}$ and $\frac{\partial u_{z_1}}{\partial y}$ are the rotations of the cross-sections, ϕ_x and ϕ_z . The problem has three unknown variables, three degrees of freedom (DOF), once this variable are found all the displacements, strains

and stresses can be obtained.

The only deformation not disregarded is the axial strain, ϵ_{yy} considering all the previous hypothesis. As it is been defined before, in Eq.1.8, the axial strain is equal to the variation of the axial displacement along y axis. Substituting the Eq.1.19 in the definition of axial strain results:

$$\epsilon_{yy}(x, y, z) = \frac{\partial v_1}{\partial y} + \frac{\partial^2 u_1}{\partial y^2} x - \frac{\partial^2 w_1}{\partial y^2} z \quad (1.24)$$

Finally applying the Hooke's law and renaming the derivatives to k_y^y , k_{yy}^z and k_{yy}^x respectively, the following equation is obtained:

$$\sigma_{yy}(x, y, z) = E(k_y^y + k_{yy}^z x k_{yy}^x z) \quad (1.25)$$

1.3.2 Timoshenko Beam Theory

The Timoshenko Beam Theory (TBT) assume the first two hypothesis of the Euler Bernoulli Beam Theory but not the last hypothesis, being the cross-section not necessary perpendicular to the neutral surface. So, differently from the EBBT, the shear stresses ϵ_{xy} and ϵ_{yz} are not negligible and the cross-section rotation around the neutral surface is not anymore equivalent to the derivatives of the axial displacement along the orthogonal axis. Now, the displacement field can be written as following:

$$\begin{aligned} u(x, y, z) &= u_1(y) \\ v(x, y, z) &= v_1(y) - x\phi_z(y) - z\phi_x(y) \\ w(x, y, z) &= w_1(y) \end{aligned} \quad (1.26)$$

Instead of three unknowns as with EBBT, TBT has five unknowns, adding the two rotations along the orthogonal axis to the three displacements. In Fig.1.5 the comparison between EBBT and TBT is shown.

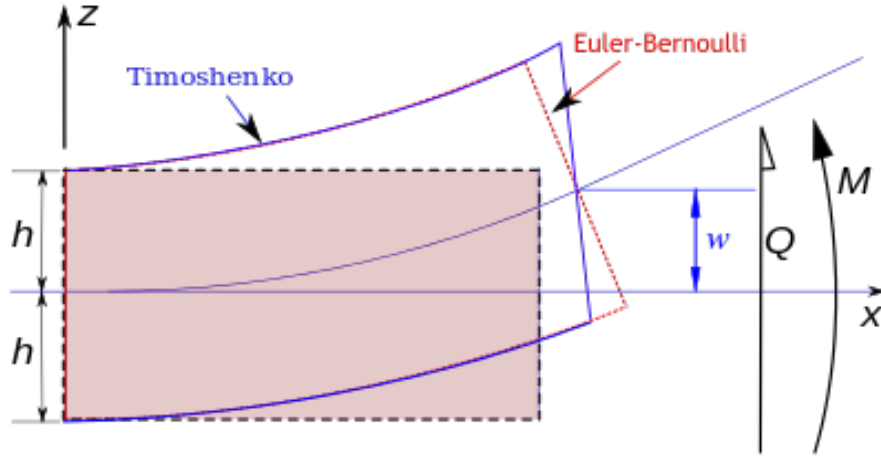


Figure 1.5: TBT vs EBBT

As the shear strains out-plane are not negligible the strain field in TBT results:

$$\begin{aligned}
 \epsilon_{yy} &= \frac{\partial v_1}{\partial y} + \frac{\partial \phi_z}{\partial y} x + \frac{\partial \phi_x}{\partial y} z \\
 \epsilon_{yz} &= \frac{1}{2} \left(\phi_z + \frac{\partial w_1}{\partial y} \right) \\
 \epsilon_{xy} &= \frac{1}{2} \left(\phi_x + \frac{\partial u_1}{\partial y} \right)
 \end{aligned} \tag{1.27}$$

Applying the Hooke's law (constitutive equation) the stresses can be obtained:

$$\begin{aligned}
 \sigma_{yy} &= E \left(\frac{\partial v_1}{\partial y} + \frac{\partial \phi_z}{\partial y} x + \frac{\partial \phi_x}{\partial y} z \right) \\
 \sigma_{yz} &= \frac{1}{2} G \left(\phi_z + \frac{\partial w_1}{\partial y} \right) \\
 \sigma_{xy} &= \frac{1}{2} G \left(\phi_x + \frac{\partial u_1}{\partial y} \right)
 \end{aligned} \tag{1.28}$$

Where E is the Young Modulus and G the shear modulus.

The shear stresses obtained by TBT don't satisfy the stress-free condition at the unloaded edges of the cross-section.

1.4 Plate theories

1.4.1 Classical plate model Kirchoff-Love

Analogous to EBBT, the classical plate model based on Kirchoff-Love hypothesis assumes three hypothesis.

1. The straight lines normal to the mid-surface remain straight after any deformation.
2. The straight lines normal to the mid-surface remain normal to the mid-surface after any deformation.
3. The thickness of the plate remains constant during the deformation.

Considering the z axis the thickness direction and the mid-plane laying in the xy -plane, the kinematic field of the Kirchoff-Love plate model can be write as following:

$$\begin{aligned}u(x, y, z) &= u_1(x, y) - z \frac{\partial w_1(x, y)}{\partial x} \\v(x, y, z) &= v_1(x, y) - z \frac{\partial w_1(x, y)}{\partial y} \\w(x, y, z) &= w_1(x, y)\end{aligned}\tag{1.29}$$

Being u_1 , v_1 and w_1 the displacements of the mid-plane. The angles between the normal to the mid-surface and z -axis ϕ_x and ϕ_y considering the third assumption can be expressed as:

$$\begin{aligned}\phi_x &= - \frac{\partial w_1}{\partial y} \\ \phi_y &= - \frac{\partial w_1}{\partial x}\end{aligned}\tag{1.30}$$

Considering the three kinematic assumptions and the relations between strains and displacements, the only strains that are not non-zero are in the in-plane directions. ϵ_{xy} can be

formulated as:

$$\epsilon_{xy}(x, y, z) = \frac{1}{2} \left(\frac{\partial u_1}{\partial y} + \frac{\partial v_1}{\partial x} \right) - z \frac{\partial w^2}{\partial x \partial y} \quad (1.31)$$

Finally, applying the Hooke's law (the constitutive equations) the shear stresses can be written as following:

$$\sigma_{xy}(x, y, z) = \frac{1}{2} G \left(\frac{\partial u_1}{\partial y} + \frac{\partial v_1}{\partial x} \right) - z G \frac{\partial w^2}{\partial x \partial y} \quad (1.32)$$

1.4.2 Reissner and Mindlin plate model

Considering the angles ϕ_x and ϕ_z not equal to the partial derivatives of the transverse displacements with respect to the in-plane coordinates x,y, the shear stresses can be taken into account. The resulting kinematic field introduced by Reissner and Mindlin is:

$$\begin{aligned} u(x, y, z) &= u_1(x, y) - z \phi_y(x, y) \\ v(x, y, z) &= v_1(x, y) - z \phi_x(x, y) \\ w(x, y, z) &= w_1(x, y) \end{aligned} \quad (1.33)$$

This plate model does not consider the effects due to thickness stretching and, as the TBT, does not satisfy the null stresses conditions at the top and bottom faces of the plate. The strain field can be formulated as:

$$\begin{aligned} \epsilon_{xy}(x, y, z) &= \frac{1}{2} \left(\frac{\partial u_1}{\partial y} + \frac{\partial v_1}{\partial x} \right) - \frac{z}{2} \left(\frac{\partial \phi_x}{\partial y} + \frac{\partial \phi_y}{\partial x} \right) \\ \epsilon_{xz}(x, y, z) &= \frac{1}{2} \left(\frac{\partial w_1}{\partial x} - \phi_x \right) \\ \epsilon_{yz}(x, y, z) &= \frac{1}{2} \left(\frac{\partial w_1}{\partial x} - \phi_x \right) \end{aligned} \quad (1.34)$$

To account for the inaccuracy in the shear strain, a correction factor, k can be applied in both ϵ_{xz} and ϵ_{yz} .

More information about the beam and plates theories can be found in [1] and [2] as well as different examples and the comparison between the beam and plates theories with the CUF theory that will be presented next.

Chapter 2

Carrera Unified Formulation - CUF theory

It is well-known that classical theories have several limitations for the study of generic structural problems. High order effect or physical inconsistencies such as torsion or in-plane deformations have to be solved with the enrichment of the kinematics, theoretically with an infinite terms. But the more terms used in the kinematics results in more complexity of the formulation and resolution of the problem.

In this Chapter the Carrera Unified Formulation is presented ([1], [2], [3], [4], [5]). This formulation solve the issues previously presented and describes the kinematic field in a unified manner that will be then exploited to derive the governing equation in a hierarchical compact way.

2.1 Displacement field for one dimensional models

The displacement field in CUF framework is described as a generic expansion of the generalized displacements by arbitrary functions. In case of **one-dimensional models** (beam models) the functions are depending of the cross-section coordinates:

$$u(x, y, z) = F_\tau(x, z)u_\tau(y) \quad \tau = 1, 2, \dots, M \quad (2.1)$$

where F_τ are the functions of the cross-section coordinates x and z , u_τ the general displacements vector and M is the number of terms in the expansion.

The discretization along y-axis of the beam is made by means of finite element method. So, the generalized displacements, u_τ , are described as functions of the unknown nodal displacement vector, $q_{\tau i}$ and the one dimensional shape functions, N_i :

$$u_\tau(y) = N_i q_{\tau i} \quad i = 1, 2, \dots, k \quad (2.2)$$

where k is the number of element nodes and the unknown nodal vector is defined as following:

$$q_{\tau i} = \left\{ \begin{matrix} q_{u_{\tau i}} & q_{v_{\tau i}} & q_{w_{\tau i}} \end{matrix} \right\}^T \quad (2.3)$$

Different sets of functions can be used to model the 1D element. In this thesis the only functions used are the Lagrange-type shape functions. Three types of Lagrange elements are considered and described. Each type has a different number of nodes in the element and consequently different polynomial degree of the functions.

Two-node B2 element

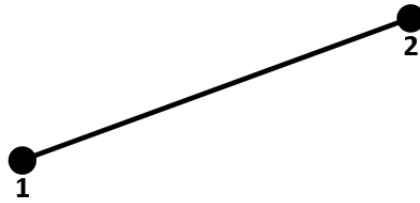


Figure 2.1: Two-node B2 element

$$N_1 = \frac{1}{2}(1 - r), \quad N_2 = \frac{1}{2}(1 + r), \quad \begin{cases} r_1 = -1 \\ r_2 = +1 \end{cases} \quad (2.4)$$

where r varies from -1 to +1 and r_i indicates the node position within the beam boundaries.

Three-node B3 element

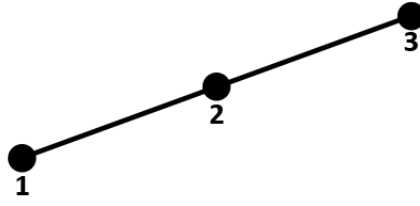


Figure 2.2: Three-node B3 element

$$N_1 = \frac{1}{2}r(1-r), \quad N_2 = \frac{1}{2}r(1+r), \quad N_3 = -(1+r)(1-r), \quad \begin{cases} r_1 = -1 \\ r_2 = +1 \\ r_3 = 0 \end{cases} \quad (2.5)$$

Four-node B4 element

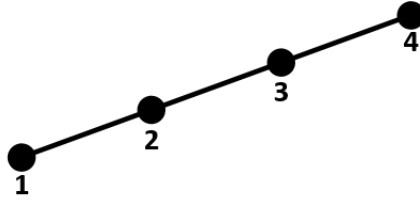


Figure 2.3: Four-node B4 element

$$\begin{aligned} N_1 &= -\frac{9}{16}(r + \frac{1}{3})(r - \frac{1}{3})(r - 1), & N_2 &= +\frac{9}{16}(r + \frac{1}{3})(r - \frac{1}{3})(r + 1), \\ N_3 &= +\frac{27}{16}(r + 1)(r - \frac{1}{3})(r - 1), & N_4 &= -\frac{27}{16}(r + 1)(r + \frac{1}{3})(r - 1), \end{aligned} \quad \begin{cases} r_1 = -1 \\ r_2 = +1 \\ r_3 = -\frac{1}{3} \\ r_4 = +\frac{1}{3} \end{cases} \quad (2.6)$$

By substituting the equation 2.2 in the equation 2.1 the displacement field results:

$$u(x, y, z) = F_\tau(x, z)N_i(y)q_{\tau i} \quad \tau = 1, 2, \dots, M \quad i = 1, 2, \dots, k \quad (2.7)$$

where M is the number of terms of the expansion and i the number of nodes for each element in the structural mesh.

About the functions of the cross-section expansion, different refined theories have been introduced. Taylor and Lagrange expansions will be next explained although in this thesis only Lagrange expansions on the beam cross-section have been used.

2.1.1 Taylor expansions

The Taylor expansion model is based in Taylor polynomials which are used as generic functions in the displacement field of the cross.section. The expansions order is introduced as an input and arbitrary. The 2D polynomials set are the type $x^i z^j$. For example, the third-order, N=3 derives into the following displacement field:

$$\begin{aligned}
u_x &= u_{x1} + xu_{x2} + zu_{x3} + x^2u_{x4} + xzu_{x5} + z^2u_{x6} + x^3u_{x7} + x^2zu_{x8} + xz^2u_{x9} + z^3u_{x10} \\
u_y &= u_{y1} + xu_{y2} + zu_{y3} + x^2u_{y4} + xzu_{y5} + z^2u_{y6} + x^3u_{y7} + x^2zu_{y8} + xz^2u_{y9} + z^3u_{y10} \\
u_z &= u_{z1} + xu_{z2} + zu_{z3} + x^2u_{z4} + xzu_{z5} + z^2u_{z6} + x^3u_{z7} + x^2zu_{z8} + xz^2u_{z9} + z^3u_{z10}
\end{aligned} \tag{2.8}$$

As it can be observed the N=3 model uses constant, linear, parabolic and quadratic generic functions. This kinematic filed is able to represent higher order effects than the classical one. This can be achieve by paying the cost of that now are 30 unknown variables for the displacement field on contrast with the five unknowns of the Thimoshenko model, for example.

The case with N=1 is known as complete linear expansion case (CLEC) and permits a linear distribution on the cross-section and the terms ϵ_{xx} , ϵ_{zz} and ϵ_{zz} which were negligible with the classical beam theories now can be accounted. The N=1 Taylor expansion displacement fields can be described as:

$$\begin{aligned}
u_x &= u_{x1} + xu_{x2} + zu_{x3} \\
u_y &= u_{y1} + xu_{y2} + zu_{y3} \\
u_z &= u_{z1} + xu_{z2} + zu_{z3}
\end{aligned} \tag{2.9}$$

The classical models, EBBT and TBT are particular cases of the N=1 model (CLEC) after applying the hypothesis for each theory mentioned before. Accounting the in-plane deformations by the CLEC leads to the detection of the torsional effects.

2.1.2 Lagrange Expansion

Lagrange expansions (LE) beam theories are based in the Lagrange polynomials, used as a generic functions above the cross-section of the beam. The cross-section is divided into a local expansion sub-domains, refining the mesh to be able to represent complex beam shapes. The polynomial degree depends on the type of Lagrange Expansion used. The more typical lagrange polynomials are three-node linear (L3), four-node bilinear (L4), nine-node cubic (L9) and sixteen-node quartic (L16). The interpolation functions and the nodes position of L3, L4 and L9 Lagrange expansion elements is next presented.

Three-node linear L3 element

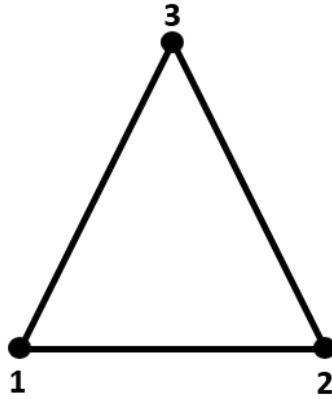


Figure 2.4: Three-node linear L3 element

The L3 element interpolation functions are given by:

$$F_1 = 1 - r - s, \quad F_2 = r, \quad F_3 = s \quad (2.10)$$

where r and s take the values -1 and +1.

Three-node linear L4 element

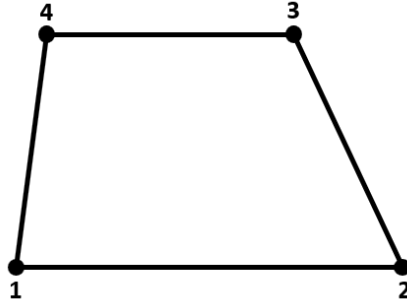


Figure 2.5: Three-node linear L4 element

$$F_\tau = \frac{1}{4}(1 + rr_\tau)(1 + ss_\tau), \quad \tau = 1, 2, 3, 4 \quad (2.11)$$

where r and s vary from -1 to +1.

Three-node linear L9 element

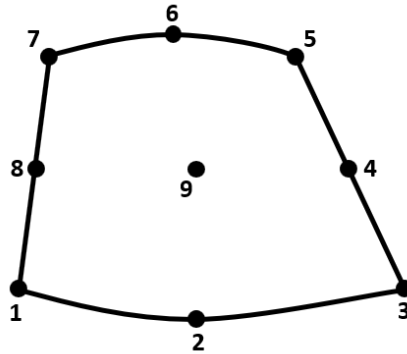


Figure 2.6: Three-node linear L9 element

$$\begin{aligned} F_\tau &= \frac{1}{4}(r^2 + rr_\tau)(s^2 + ss_\tau), \quad \tau = 1, 3, 5, 7 \\ F_\tau &= \frac{1}{2}s_\tau^2(s^2 + ss_\tau)(1 - r^2) + \frac{1}{2}r_\tau^2(r^2 + rr_\tau)(1 - s^2), \quad \tau = 2, 4, 6, 8 \\ F_\tau &= (1 - r^2)(1 - s^2), \quad \tau = 9 \end{aligned} \quad (2.12)$$

where r and s vary from -1 to +1. The displacement field above the cross-section for the L9

element results:

$$\begin{aligned}
u_x &= F_1 u_{x1} + F_2 u_{x2} + F_3 u_{x3} + F_4 u_{x4} + F_5 u_{x5} + F_6 u_{x6} + F_7 u_{x7} + F_8 u_{x8} + F_9 u_{x9} \\
u_y &= F_1 u_{y1} + F_2 u_{y2} + F_3 u_{y3} + F_4 u_{y4} + F_5 u_{y5} + F_6 u_{y6} + F_7 u_{y7} + F_8 u_{y8} + F_9 u_{y9} \\
u_z &= F_1 u_{z1} + F_2 u_{z2} + F_3 u_{z3} + F_4 u_{z4} + F_5 u_{z5} + F_6 u_{z6} + F_7 u_{z7} + F_8 u_{z8} + F_9 u_{z9}
\end{aligned} \tag{2.13}$$

By adopting higher order Lagrange polynomials refined beam models can be obtained. Also a combination of Lagrange polynomials on multi-domain cross-section are used to refine some models.

2.2 Displacement field for two dimensional models

The displacement field for plates two dimensional models can be described as following:

$$u(x, y, z) = F_\tau(z)u_\tau(x, y) \quad \tau = 1, 2, \dots, M \tag{2.14}$$

This displacement field differs from the beam displacement field as now the generalized displacement are function of the mid-plane coordinates of the plate and the expansion mesh is in the thickness direction (z-axis).

So, now, the expansion mesh is one dimensional in the thickness direction. The expansion functions F_τ now depends only on the z coordinate meanwhile the generalized displacements $u_\tau(x, y)$ depends on x and y coordinates.

The expansion functions F_τ can be model as Lagrange polynomials like the one dimensional functions for the generalized displacements for the beam ($N_{\tau i}$). B2, B3 and B4 elements are considered. This functions can also be model using Taylor polynomials.

The generalized displacements, u_τ are described as functions of the unknown nodal displacements vector, $q_{\tau i}$ and the two dimensional shape functions, N_i . This functions that only depend on y coordinate in beam models, in plate depend on x and y coordinate, the mid-plane coordinates of the plate.

$$u_\tau(x, y) = N_i(x, y)q_{\tau i} \quad i = 1, 2, \dots, k \tag{2.15}$$

So, analogously to the beam the displacement field of a plate results:

$$u(x, y, z) = F_\tau(z)N_i(x, y)q_{\tau i} \quad \tau = 1, 2, \dots, M \quad i = 1, 2, \dots, k \quad (2.16)$$

where M is the number of terms of the expansion (i.e the number of nodes for each element in the expansion) and i the number of nodes used for each element in the structural mesh.

2.3 Governing equation and stiffness matrix

The governing equations are derived by the principle of virtual displacements, PVD. In this section only the static analysis will be accounted for the deduction of the governing equations as all the examples been carried on in this thesis are analysed statically. For the sake of simplicity the governing equations are only derived for the beam, but the same process can be done to obtain the governing equations of a plate.

The principle of virtual displacements states that to have equilibrium in a structure the necessary condition is that the virtual variation of the internal work has to be equal to the virtual variation of the external work, so:

$$\delta L_{int} = \delta L_{ext} \quad (2.17)$$

The internal work can be defined as equivalent to the elastic strain energy:

$$\delta L_{int} = \int_l \int_\Omega \delta e^T \sigma d\Omega dy \quad (2.18)$$

where l stands for the length of the beam and Ω for the cross-section area. The internal work can also be divided in to two parts, the in-plane actions, L_{int}^Ω and the normal actions, L_{int}^n . This results:

$$\delta L_{int} = \int_l \int_\Omega \delta e_\Omega^T \sigma_\Omega d\Omega dy + \int_l \int_n \delta e_n^T \sigma_n d\Omega dy \quad (2.19)$$

By considering the geometrical relation (1.12), the constitutive law (1.14), the CUF kin-

matic field (2.1) and the FEM discretization (2.2), the internal work can be rewritten as:

$$\begin{aligned}
\delta L_{int} = & \int_l \delta \mathbf{q}_{\tau i}^T N_i \left[\int_{\Omega} (\mathbf{D}_{\Omega n}^T F_{\tau} \mathbf{I}) C_{\Omega n} (\mathbf{D}_{nn} F_s \mathbf{I}) d\Omega \right] N_j \mathbf{q}_{sj} dy + \\
& + \int_l \delta \mathbf{q}_{\tau i}^T N_i \left[\int_{\Omega} (\mathbf{D}_{\Omega n}^T F_{\tau} \mathbf{I}) C_{\Omega \Omega} (\mathbf{D}_{\Omega n} F_s \mathbf{I}) d\Omega \right] N_j \mathbf{q}_{sj} dy + \\
& + \int_l \delta \mathbf{q}_{\tau i}^T N_i \left[\int_{\Omega} (\mathbf{D}_{\Omega n}^T F_{\tau} \mathbf{I}) C_{\Omega \Omega} F_s d\Omega \right] \mathbf{I}_{\Omega y}^T N_{j,z} \mathbf{q}_{sj} dy + \\
& + \int_l \delta \mathbf{q}_{\tau i}^T N_i \left[\int_{\Omega} (\mathbf{D}_{nn}^T F_{\tau} \mathbf{I}) C_{nn} (\mathbf{D}_{nn} F_s \mathbf{I}) d\Omega \right] N_j \mathbf{q}_{sj} dy + \\
& + \int_l \delta \mathbf{q}_{\tau i}^T N_i \left[\int_{\Omega} (\mathbf{D}_{nn}^T F_{\tau} \mathbf{I}) C_{n\Omega} (\mathbf{D}_{\Omega n} F_s \mathbf{I}) d\Omega \right] N_j \mathbf{q}_{sj} dy + \\
& + \int_l \delta \mathbf{q}_{\tau i}^T N_i \left[\int_{\Omega} (\mathbf{D}_{nn}^T F_{\tau} \mathbf{I}) C_{n\Omega} F_s d\Omega \right] \mathbf{I}_{\Omega y}^T N_{j,z} \mathbf{q}_{sj} dy + \\
& + \int_l \delta \mathbf{q}_{\tau i}^T N_i \left[\int_{\Omega} F_{\tau} C_{\Omega n} (\mathbf{D}_{nn} F_s \mathbf{I}) d\Omega \right] N_j \mathbf{q}_{sj} dy + \\
& + \int_l \delta \mathbf{q}_{\tau i}^T N_i \left[\int_{\Omega} F_{\tau} C_{\Omega \Omega} (\mathbf{D}_{\Omega n} F_s \mathbf{I}) d\Omega \right] N_j \mathbf{q}_{sj} dy + \\
& + \int_l \delta \mathbf{q}_{\tau i}^T N_i \left[\int_{\Omega} F_{\tau} C_{\Omega \Omega} F_s \mathbf{I} d\Omega \right] \mathbf{I}_{\Omega y}^T N_{j,z} \mathbf{q}_{sj} dy
\end{aligned} \tag{2.20}$$

Introducing the stiffness matrix of the finite element, the previous expression can be compacted as:

$$\delta L_{int} = \delta \mathbf{q}_{\tau i}^T \mathbf{K}^{\tau sij} \mathbf{q}_{sj} \tag{2.21}$$

where $K^{\tau sij}$ is the fundamental nucleus of the stiffness matrix. The nine terms of this matrix are formulated below:

$$\begin{aligned}
K_{xx}^{\tau sij} &= C_{22} \int_l N_i N_j dy \int_{\Omega} F_{\tau,x} F_{s,x} d\Omega + C_{44} \int_l N_i N_j dy \int_{\Omega} F_{\tau,z} F_{s,z} d\Omega \\
&\quad + C_{66} \int_l N_{i,y} N_{j,y} dy \int_{\Omega} F_{\tau} F_s d\Omega \\
K_{xy}^{\tau sij} &= C_{23} \int_l N_i N_{j,y} dy \int_{\Omega} F_{\tau} F_{s,x} d\Omega + C_{66} \int_l N_{i,y} N_j dy \int_{\Omega} F_{\tau,x} F_s d\Omega \\
K_{xz}^{\tau sij} &= C_{12} \int_l N_i N_j dy \int_{\Omega} F_{\tau,z} F_{s,x} d\Omega + C_{44} \int_l N_i N_j dy \int_{\Omega} F_{\tau,x} F_{s,z} d\Omega \\
K_{yx}^{\tau sij} &= C_{23} \int_l N_{i,y} N_j dy \int_{\Omega} F_{\tau,x} F_s d\Omega + C_{66} \int_l N_i N_{j,y} dy \int_{\Omega} F_{\tau} F_{s,x} d\Omega \\
K_{yy}^{\tau sij} &= C_{33} \int_l N_{i,y} N_{j,y} dy \int_{\Omega} F_{\tau} F_s d\Omega + C_{55} \int_l N_i N_j dy \int_{\Omega} F_{\tau,z} F_{s,z} d\Omega \\
&\quad + C_{66} \int_l N_i N_j dy \int_{\Omega} F_{\tau,x} F_{s,x} d\Omega \\
K_{yz}^{\tau sij} &= C_{13} \int_l N_{i,y} N_j dy \int_{\Omega} F_{\tau,z} F_s d\Omega + C_{55} \int_l N_i N_{j,y} dy \int_{\Omega} F_{\tau} F_{s,z} d\Omega \\
K_{zx}^{\tau sij} &= C_{12} \int_l N_i N_j dy \int_{\Omega} F_{\tau,x} F_{s,z} d\Omega + C_{44} \int_l N_i N_j dy \int_{\Omega} F_{\tau,z} F_{s,x} d\Omega \\
K_{zy}^{\tau sij} &= C_{13} \int_l N_i N_{j,y} dy \int_{\Omega} F_{\tau} F_{s,z} d\Omega + C_{55} \int_l N_{i,y} N_j dy \int_{\Omega} F_{\tau,z} F_s d\Omega \\
K_{zz}^{\tau sij} &= C_{11} \int_l N_i N_j dy \int_{\Omega} F_{\tau,z} F_{s,z} d\Omega + C_{44} \int_l N_i N_j dy \int_{\Omega} F_{\tau,x} F_{s,x} d\Omega \\
&\quad + C_{55} \int_l N_{i,y} N_{j,y} dy \int_{\Omega} F_{\tau} F_s d\Omega
\end{aligned} \tag{2.22}$$

where the constants C_{ij} stand for the material stiffness coefficients.

The external work will be defined as:

$$\delta L_{ext} = \delta \mathbf{q}^T \mathbf{P} \tag{2.23}$$

where \mathbf{P} is the loading vector. Introducing this equation and the definition of the internal work in Eq.2.17 the algebraic system to be solved results:

$$\mathbf{K} \mathbf{q} = \mathbf{P} \tag{2.24}$$

In Fig.2.7, Fig.2.8 and Fig.2.9 the assembly procedure of the stiffness matrix is shown. The stiffness matrix is built from the pairs of indexes τ, s and i, j . The first two indexes refer to the expansion functions on the cross-section, meanwhile the i, j indexes refer to the structural element mesh. So, for each structural node there is a $\tau - s$ sub-matrix. This

matrix is created by assembling the \mathbf{K} fundamental nucleus. This matrix is shown in Fig.2.7.

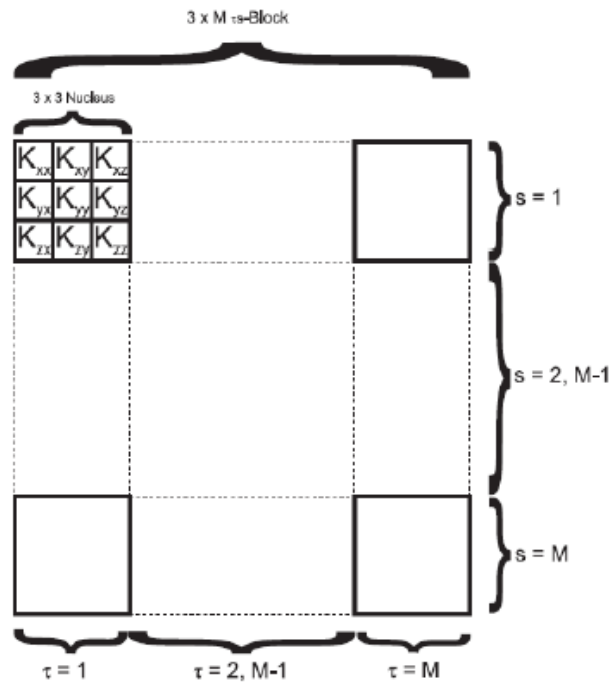


Figure 2.7: Assembly of the $\tau - s$ sub-matrix

In order to create the i - j sub-matrices the matrices $\tau - s$ of each node of the structural elements are assembled. So, each matrix i - j represent each of the structural elements of the structure. This assembly is shown in Fig.2.8

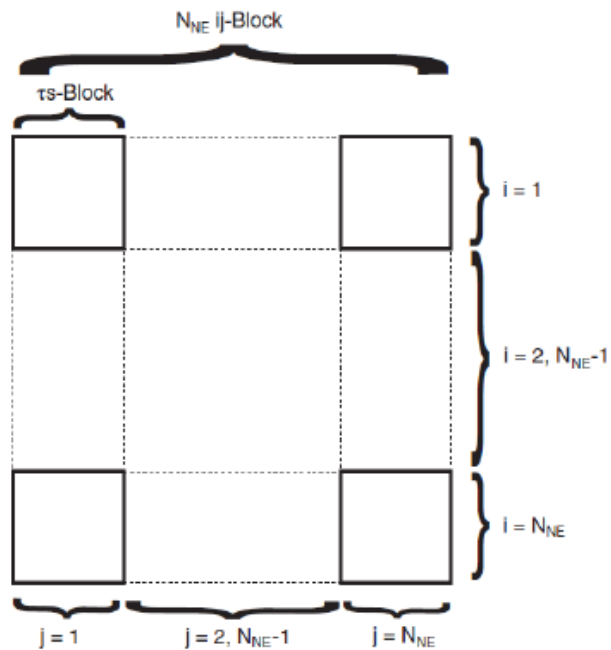


Figure 2.8: Assembly of the $i - j$ sub-matrix

Finally, assembling the i - j matrices the global stiffness matrix is created as it is displayed

in Fig.2.9 . The dimension of the global stiffness matrix will be (x,x) being x the number of degrees of freedom (DOF's) of the entire model.

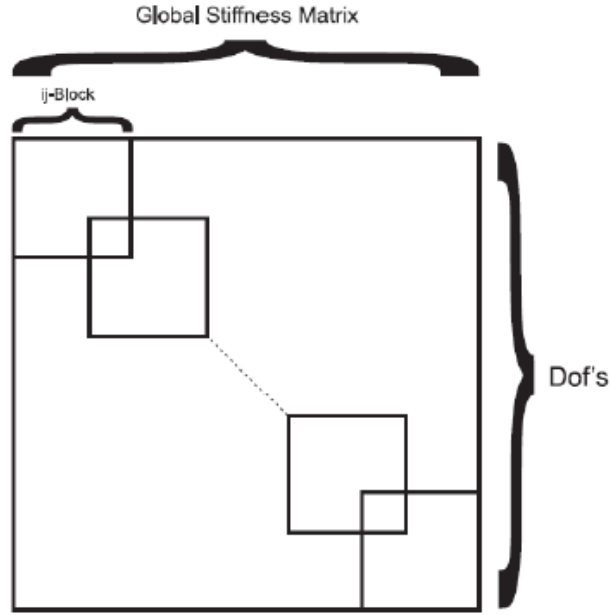


Figure 2.9: Assembly of the global stiffness matrix

2.4 Loading vector

In all the examples of the thesis only point loads have been considered so in this section, this type of loads will be explained. The generic components of a point load can be represented with the following vector:

$$\mathbf{F} = [F_x, F_y, F_z] \quad (2.25)$$

The virtual work of a generic force can be defined as:

$$\delta L_{ext} = \delta \mathbf{u}^T \mathbf{F} \quad (2.26)$$

where δu are the virtual displacement resultants of the point load. Introducing the finite element discretization and the nodal displacements and the CUF shape functions notation this equation is written as:

$$\delta L_{ext} = \delta \mathbf{q}_{\tau i}^T F_{\tau} N_i \mathbf{F} \quad (2.27)$$

Reagrouping the longitudinal shape functions and the expansion functions with the force

vector results:

$$\delta L_{ext} = \delta \mathbf{q}_{\tau i}^T P^{\tau i} \quad (2.28)$$

where P is the loading vector.

Chapter 3

Composite materials

Nowadays composite materials are extremely common in many engineering applications. Concrete and wood, for example are composite materials. A composite material is made from two or more materials with different physical or chemical properties. When this two materials are combined they produce a material with different characteristics than both. The individual components remain separate in the final structure and can be distinct contrasting composites from mixtures or solid solutions where the different materials can not be distinct in the final structure. The new material will be preferred than the individual ones having more strength, being lighter or less expensive between other reasons.

For example considering concrete, it's very strong if you use it in vertical beams to support the weight of a building or a structure (compression) but it's weak and tends to bow and snap if it's used horizontally (in tension). A great an usual solution is to pour wet concrete around tight steel bars (rebars) that results into a composite material called reinforced concrete. This steel bars pulls on the concrete to stop it snapping when it's under tension, while the concrete protects the steel from rust and decay. The result is a composite material that works well under tension and compression.

The most common reason for making a composite is adding strength, but it is not the only one. Other examples of properties that someone would like to improve could be fatigue resistance (for example in a part of an airplane that it is repeatedly stressed and strained during flight), tolerance at higher temperatures (for example in an engine part), more stiffness keeping a material lightweight, carry heat and electricity better etc.

3.1 Composite materials in aeronautics

Composite materials have been used in aeronautics many years. The benefits of exploiting the excellent specific strength and stiffness properties of composites, specially for lightweight structural design are very transcendental.

The composites took-off in aircraft in 1909 with the invention of phenolic resin. The most famous example of the first composites aircrafts was the deHavilland Albatross manufactured from a sandwich fuselage construction. This aircraft was later developed into the deHavilland Mosquito (a combat aircraft for the second world war). Mosquito had wooden construction with fibres made of phenolic resins that made it extremely light, fast and agile and cheaper than its metallic counterparts. In the Fig.3.1 both deHavilland models are shown.



(a) DeHavilland Albatross, *Source: Wikipedia*



(b) DeHavilland Mosquito, *Source: bomber-commandmuseum.ca*

Figure 3.1: Examples of deHavilland Albatross and Mosquito

Since the development of carbon and glass fibres in the 1950's the aerospace industry is moving to all-composite aircrafts. Nowadays the most common fibres used are glass, carbon, aramid-kevlar and the most resin types used are phenolic, polyester and epoxy:

- **Glass fibres** are used specially in boats and doesn't have high strength or stiffness.
- **Carbon fibres** are highly used in aerospace being more strength and stiff than glass ones but more expensive.
- **Aramid-kevlar fibres** have more or less the same strength than glass fibres but a bit more of stiffness. Their use in aerospace is less than carbon fibres (sometimes for impact protection on aircraft) and are more suitable for bullet-proof vests, helmets etc.
- **Phenolic resin** is used in aircraft interiors because it have a good chemical, heat and

fire resistance although it tends to be brittle.

- **Polyester resin** is more used in boats, wind turbine blades and other cost critical operations. It's tougher than phenolic but it burns very easily.
- **Epoxy resin** is used in combination with carbon fibres for high performance lightweight applications such as aircrafts being the most common resin in aerospace. It has good chemical resistance and it can be made quite tough.

The change from metallic to composite construction has also induced a change in the design and methodology of aircraft components due to the difference between mechanical physical and chemical properties between metallic and composites. For example, the failure modes in composites are very different and can be a fibre or resin failure, debonding, delamination, etc. That, generally, increases the analytical workload and sometimes these failures are more difficult to exactly predict.

The first generation of commercial aircrafts that contain large proportion parts made of composite materials, such as the Boeing 787 Dreamliner and Airbus A350 XWB (Fig.3.2), are doing regular flights for a few years. The composite materials enable the designer to tailor optimum mechanical properties by orientating the direction of the fibre with the primary load paths. Reinforcing the fibres has other advantages like ease to manufacture complex shapes and excellent fatigue and corrosion resistance.



(a) Boeing 787 Dreamliner *Source: boeing.com*



(b) Airbus A350 XWB *Source: airbus.com*

Figure 3.2: First commercial aircrafts with large proportion of composite materials

3.2 Composite laminates

A composite laminate material is a composite material where each material compose a layer. These layers are bonded together using resin in the thickness direction. Each layer made of different material could consist of short fibres, unidirectional continuous fibres or also woven fibres embedded in a matrix. Controlling the orientation of fibres in each laminate the properties of the composite laminate can be altered and more strength, durability or some other benefits can be achieved. A composite laminate example is shown in Fig.3.3

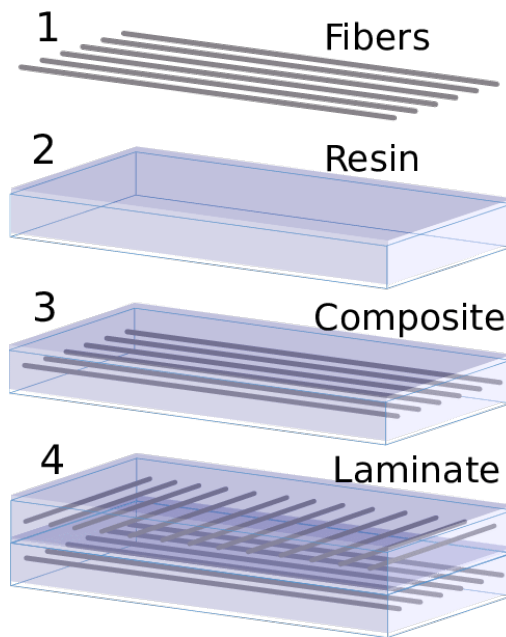


Figure 3.3: Example of a composite laminate

Usually the composite is made symmetrically. The ply orientation is symmetrical about the mid plane of the laminate, so, for each ply above the mid-plane, there is an identical ply (in material, fibre orientation angle and thickness) at an equal distance below the mid-plane. This can be write with the following expression:

$\theta(z) = -\theta(z)$ where z is the distance from the mid-plane of the laminate.

3.3 CUF formulation for composite laminates

In this section the CUF formulation for composite laminates beams and plates is presented. Notice that only Lagrange polynomials for both structural and expansion mesh have been used during this thesis, so the CUF assembly for beams and plates composite laminates is explained for this type of expansions.

3.3.1 Beam models

Consider a generic beam model like the one shown in Fig.3.4 with three different layers. The structural mesh takes place in the y-longitudinal axis of the beam meanwhile the cross-section of the beam relays in the plane x-z where the different layers have to be taken in account.

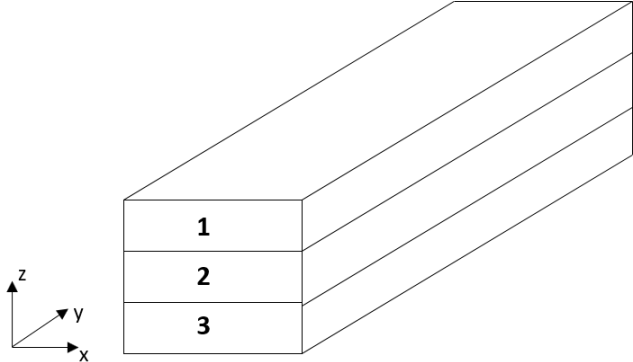


Figure 3.4: Generic composite laminate beam

Structural mesh

About the structural mesh, Lagrange polynomials B2, B3, B4 (or higher order if needed) can be used. In Fig.3.5 the beam previously proposed is described by two B3 elements. In each of the nodes an expansion in the x-z will be done.

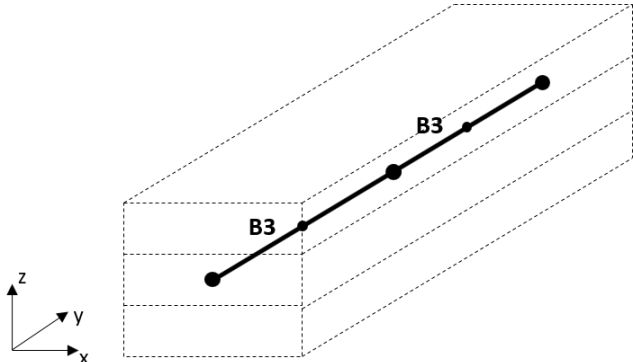


Figure 3.5: Structural mesh - 2B3

Expansion mesh

The expansion mesh can be designed with the different Lagrange expansions described in chapter 2. In this case, one L9 element per layer has been considered as it is displayed in Fig.3.6.

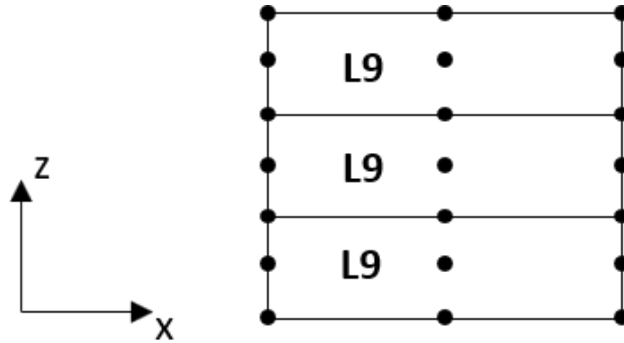


Figure 3.6: Expansion mesh - 1L9 per layer

The assembly of the stiffness matrix can be done through two different methods. The equivalent single layer and the layer wise. This two methods are shown in Fig.3.7. The first one is basically used for Taylor expansions and sums the contributions of each single layer into an unique equivalent one. As in this thesis only LE have been considered the method used is the Layer wise (LW). This method maintain the different properties of each single layer and join them in the interface.

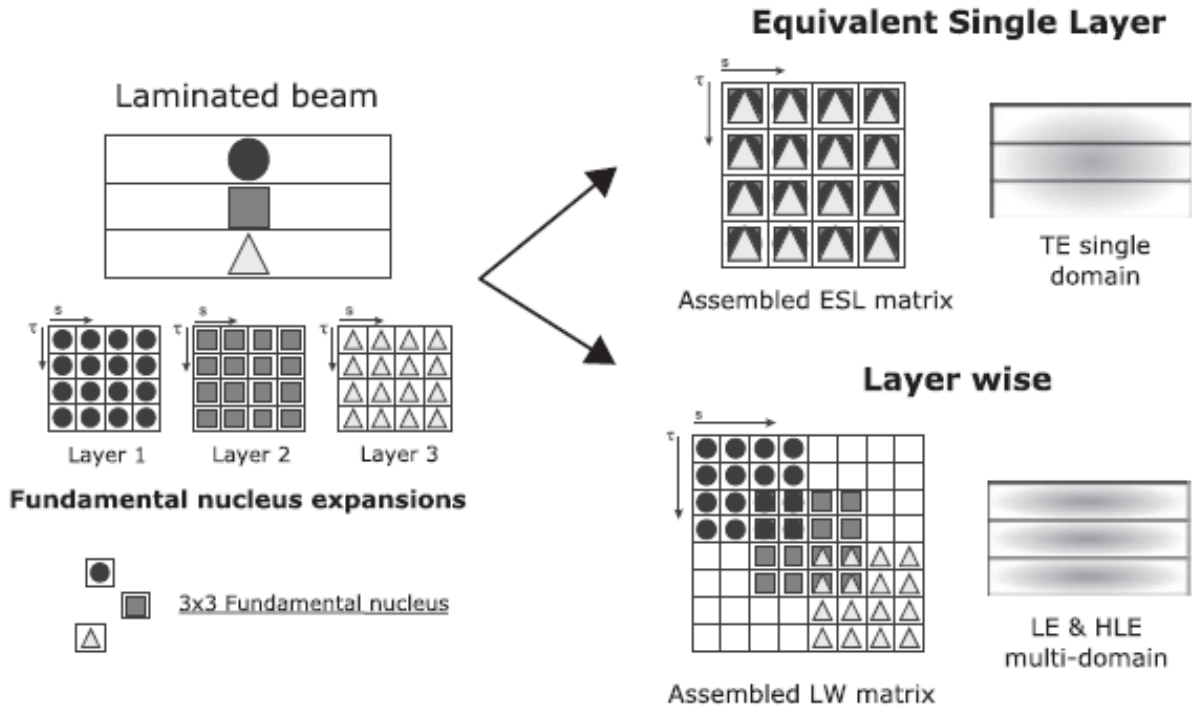


Figure 3.7: Assembly procedure of the stiffness matrix through ESL and LW approaches, *Source:* [6]

3.3.2 Plate models

Now, consider a generic composite laminate plate with three different layers as it is shown in Fig.3.8. In this case, the structural mesh is formed by the x-y plane and the expansion mesh takes place in the thickness direction (z - coordinate).

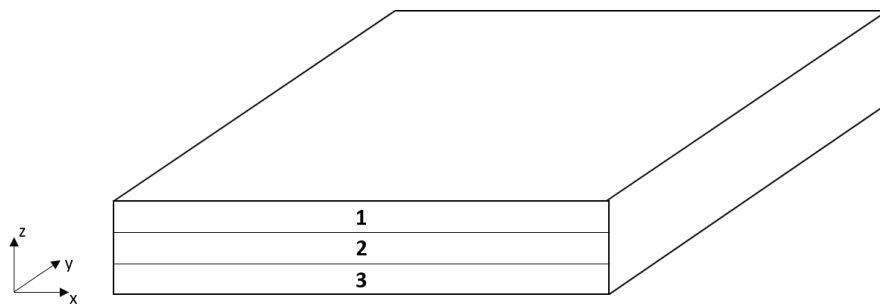


Figure 3.8: Generic composite laminate plate

Structural mesh

So the structural mesh is considered in the x-y plane. Analogously for the beam the polynomials used to create the structural mesh are the Lagrangian ones, like for example the mesh

structure Fig.3.9 where a Lagrangian polynomial of ninth order is used (Like before with the expansion cross-section, other orders can also be used and are explained in chapter 2). For each node of the structural mesh and expansion in the thickness direction (z) will be done.

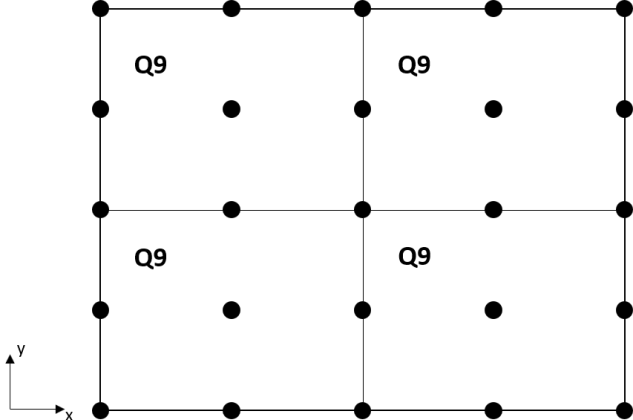


Figure 3.9: Structural mesh - 4Q9

Expansion mesh

Analogously of the structural mesh of the beam model, in the plate expansion mesh, Lagrange polynomials of order B2, B3, B4 etc can be used. In this case (Fig.3.10) one B3 element per layer is considered.

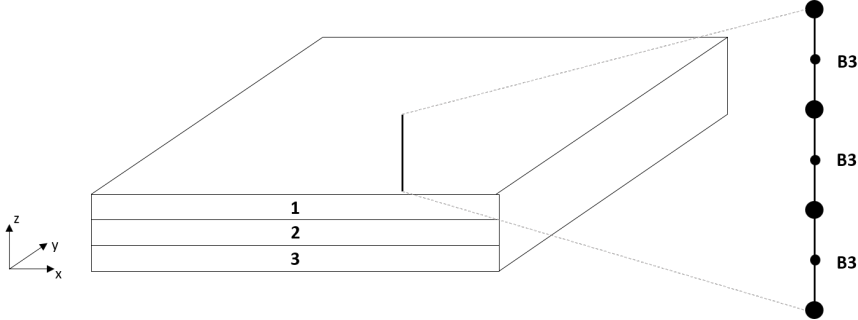


Figure 3.10: Expansion mesh - 1B3 per layer

Chapter 4

Mul2 code

In this chapter the Multilayered structures code is presented. As it is said before nowadays multilayered structures are being extensively used in a huge different engineering fields such as aerospace, automotive or civil engineering. As the classical structural analysis tools (which are available in commercial software like Ansys, Nastran etc) are not good enough to predict the behaviour of this type of structures, the MUL2 project has been developed by the Mul2 search group at PoliTO guided by Erasmo Carrera ([7]). This project is dedicated to the development of an advanced structural model for multilayered structures with particular attention to the multi-field analysis and the fluid-structure interactions. The software is based in the Carrera Unified Formulation (CUF) and works for beams, plates and shells. The Mul2 tool has been applied in different fields and applications like aeroelasticity, aircrafts design, biomechanics, composites, damage and failure, multifield analysis, rotor-dynamics among others.

During the thesis the Mul2 code has been used as a tool to perform the analysis of different models and structures. This chapter doesn't pretend to enter inside how the software works or the different capabilities of it. Instead how the software is used to perform beam and plate structural analysis is presented.

The software read 12 input files where all the inputs of the problem are defined. Once the input files are read by the software, the analysis is performed and finally a post-processor file is created. This file can be open with different post-processor software in order to visualize all the displacements, stresses or others field that wanted to be studied.

The 12 input files where the problem is described are next explained. An important thing to take into account is that the first number of the file correspond to the lines that the software will read.

File ANALYSIS

In this file the type of the analysis that will be carried out is defined. To perform a static analysis as all the cases in this thesis, the file has to begin with 101 as it can be seen in Fig.4.1 Also a coefficient correction named sheral locking correction beam can be activated, but it is not necessary for the problems exposed during this work.

```
101                !101 = STATIC, 105 = BUCKLING

100

10      Number of Modes for the Modal Analysis (** ATTENTION to ALL Modes choise)

NONE      Sheral locking correction beam (NONE/REDI/SELI/MITC)
NONE      Sheral locking correction beam (NONE/REDI/SELI/MITC)
NONE      Sheral locking correction beam (NONE/REDI/SELI/MITC)
```

Figure 4.1: Example of an analysis input file

File INFO MODEL

As it is shown in Fig.4.2 this file provides information about the case study, the sides to be studied, no sub-domains in plane and out-plane and the number of elements. This file is only informative and do not plays a role in the analysis by the software Mul2.

```
2      !Case study
3      !Case sides
4      !X subdomains
2      !Z subdomains x layer
8      !Number of B4 elements
```

Figure 4.2: Example of an info model file

File VERSORS

The file versors defines the versors used to orientate the local reference system of the elements. The four numbers to be defined are the ID and the X, Y and Z components of the versor in the global reference system. This versors will be used in the connectivity file to orientate the elements in the space. An example of this file is displayed in Fig.4.3.

```
1      N_VER = total number of versors

VERSOR  1  0  1  0
```

Figure 4.3: Example of a versors file

File MATERIAL

In this file the material and its properties are defined. In Fig.4.4 an example of this file is displayed. Isotropic or orthotropic material can be defined. Young, shear modulus and poisson coefficient⁵ have to be provided. Thermal, magnetic, electric or other properties can also be defined but they have no interest in this project.

```
1 1 N_MAT = total number of materials
ISO-M 1 7509 0.33 2700

ISO-M ID E v rho
ORT-M ID ELL ELZ ELT vLT vLZ vTZ GLT GLZ GTZ rho
```

Figure 4.4: Example of a material file

File LAMINATION

If the part or structure to be analyzed contains composites laminates, the different layers have to be defined. An example is shown in Fig.4.5. The second column indicates the ID of the layer, the third the material to be considered in this layer (previously all the materials had to be defined in the material file), next the rotation around y-axis of the layer and last the rotation around z axis.

```
4 N_LAM = total number of laminations
LAM2 1 1 0.00D+00 0.00D+00
LAM2 2 2 0.00D+00 9.00D+01
LAM2 3 1 0.00D+00 -4.50D+01
LAM2 4 1 0.00D+00 4.50D+01
```

Figure 4.5: Example of a lamination file

File NODES

The structural mesh is defined in this file. Notice that if the case to study is a beam the structural mesh will be in the plane x-z, instead if a plate is been studied the structural mesh will be the x-y plane. The first column is the node ID, the next columns the position in the space of the node, the following the kinematic model (Lagrange expansion, Taylor expansion, Legendre expansion or miscellaneous expansion) that in this thesis is always Lagrange expansion and the last one the order of the expansion defined before. An example is been displayed in Fig.4.6.

```

9
1      3.70000000D-01    4.80000000D-01    0.00000000D+00    LE 1
2      3.70669873D-01    4.80000000D-01    0.00000000D+00    LE 1
3      3.71339746D-01    4.80000000D-01    0.00000000D+00    LE 1
4      3.75669873D-01    4.80000000D-01    0.00000000D+00    LE 1
5      3.80000000D-01    4.80000000D-01    0.00000000D+00    LE 1
6      3.84330127D-01    4.80000000D-01    0.00000000D+00    LE 1
7      3.88660254D-01    4.80000000D-01    0.00000000D+00    LE 1
8      3.89330127D-01    4.80000000D-01    0.00000000D+00    LE 1
9      3.90000000D-01    4.80000000D-01    0.00000000D+00    LE 1

```

Figure 4.6: Example of a nodes file

File EXP MESH 01

The file EXP MESH 01 contains the expansion mesh of the part. There is a 01 number because it is possible to have more than 1 expansion mesh file although all the problems studied in this thesis only have one expansion mesh file. So, here the expansion mesh is defined, this is the x and y coordinates if the case studied is a beam or the z coordinate in case the part is a plate. An example of a plate expansion mesh is shown in Fig.4.7.

```

9
1      0.00000000D+00    0.00000000D+00    -1.20000000D-03
2      0.00000000D+00    0.00000000D+00    -1.16666667D-03
3      0.00000000D+00    0.00000000D+00    -1.13333333D-03
4      0.00000000D+00    0.00000000D+00    -1.10000000D-03
5      0.00000000D+00    0.00000000D+00    -1.06666667D-03
6      0.00000000D+00    0.00000000D+00    -1.03333333D-03
7      0.00000000D+00    0.00000000D+00    -1.00000000D-03
8      0.00000000D+00    0.00000000D+00    -9.66666667D-04
9      0.00000000D+00    0.00000000D+00    -9.33333333D-04

```

Figure 4.7: Example of an expansion mesh file

File CONNECTIVITY

The file connectivity provides the type of element to be used in the structural mesh and the connection between the nodes in each element. So in the first column the type of element (Q3, Q4, Q9, Q16, B3, B4 etc) to be used is defined, then the ID of the element following the nodes in order that form that element. The last two columns are the versor taken into account and the expansion that has to be used in the element.

```

4
Q9  1    1 2 3 12 21 20 19 10 11    1    1
Q9  2    3 4 5 14 23 22 21 12 13    1    1
Q9  3    5 6 7 16 25 24 23 14 15    1    1
Q9  4    7 8 9 18 27 26 25 16 17    1    1

```

Figure 4.8: Example of a connectivity file

File EXP CONN 01

Analogously with the previous file, this file contains the type and connectivity of the elements used in the expansion mesh with the difference that in the third column the layer in which the element is located has to be provided. There is an example of this file in Fig.4.9.

```

3
B4  1    1    1 2 3 4
B4  2    1    4 5 6 7
B4  3    2    7 8 9 10

```

Figure 4.9: Example of an expansion connectivity file

File BC

The boundary conditions of the problem are defined in this file. Both loads and constraints are introduced in this file. D-POINT and D-PLANE are used to impose displacements in a node or in a plane and F-POINT to impose a force in a node. Other boundary conditions like pressure, temperature, voltage etc can be also imposed but have not interest in this project. There is an example of this file in Fig.4.10. In the case of a plane constraint, the first number is the ID, the next four numbers are the coefficients A, B, C and D of the plane equation and the three last inputs are if the plane is fixed (0) or free (N) in the X, Y and Z directions respectively. Same for the D-POINT constraint replacing the equation of the plane by the X, Y and Z position of the point. Finally for the F-POINT the first column is the ID, the three following the X, Y and Z position of the point and the last three columns the value of the force in vectorial mode (X, Y and Z components).

```

3
D-PLANE  1    0.0D0  1.0D0  0.0D0  0.0D0  0.0D0  0.0D0  0.0D0  N
D-POINT  2    0.0D0  0.0D0  0.4D0  0.0D0  0.0D0  0.0D0  0.0D0
F-POINT  3    0.0D0  20.0D0 -0.4D0  0.0D0  0.0D0  0.0D0  1.0D0

```

Figure 4.10: Example of a boundary conditions file

File PBC

This file contains the number of periodical boundary conditions but it will not be explained as it is not used in all the thesis.

File POSTPROCESSING

The last file is the postprocessing file. This file contains the postprocessing information. PARA indicates that the postprocessing file that the software MUL2 will create is a paraview file. It can be replace by GMESH creating a GMESH file. With the comand PNT plus the id and the position the software will create a file with all the information about this point. An example of the file is displayed in Fig.4.11.

```

2
PARA 8 GLB 2 3 2 2 2 2 1 1 1
PNT 1 0 0 0
PARA 20 GLB 2 3 2 1 1 1 1 1 1

```

Figure 4.11: Example of a postprocessor file

Chapter 5

Global Local Analysis

In this chapter the global/local methodology through the Carrera Unified Formulation is presented ([4], [8], [9], [10]). The global/local approach is useful in case of complex and localized stress fields in aircraft structure models. Specially in case of laminates composites where commercial software 2D analysis can lead to an error specially in the out-plane stresses and free edges. The local/global approach can approximate well this type of stresses and making the analysis computationally more efficient than the solid models generally required to capture this stress fields.

This work around the global local analysis has been studied in collaboration with Embraer SA, a Brazilian aerospace conglomerate that produces commercial, military, executive and agricultural aircrafts and also provides aeronautical services. Embraer SA is the third largest producer of civil aircraft (after Boeing and Airbus). PoliTO and Embraer SA have a collaboration deal focus in the structural analysis of the aircraft that implies the studying of the global local approach through the CUF.

The global models are simulated using 1D, 2D or a combination of both finite elements with commercial software (Nastran has been used in this thesis). These models have low computational costs but as it is said they cannot capture satisfactory complex stress fields due to the kinematic assumptions of the 1D/2D finite elements. Although these models are not accurate the critical regions of the global model can be identified and then a local analysis with the CUF can be performed in these regions, detecting those complex stress fields with a high accuracy and low computational cost (Fig.5.1). To do the local analysis the boundary conditions (BCs) for the local model have to be extracted from the Nastran global model.

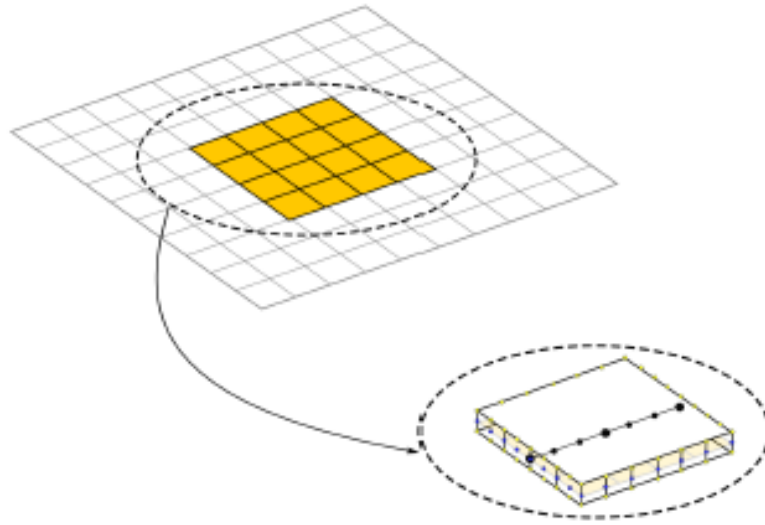


Figure 5.1: Global local model

5.1 Application of the boundary conditions

There are two types of boundary conditions for the local model, mechanical BC's and geometrical BC's.

Mechanical boundary conditions

If forces or moments are applied at the interface of the local model the static problem becomes indeterminate and the structure is unconstrained. Consequently, the stiffness matrix is singular. This problem is usually solved by a procedure known as *Inertia relief*. In this thesis no mechanical boundaries had to be applied and the *Inertia relief* procedure is not explained. Even though this approach can be found in [11] and [12].

Geometrical boundary conditions

Contrary to the mechanical BC's, the geometrical BC's, i.e the displacements and rotations at interface do not require any exceptional procedure as the system is constrained. That results to a determinate problem that can be solved. In the majority of the global/local approaches the geometrical BC's are used instead of the mechanical ones.

Fig.5.2 displays how the geometrical boundary conditions are calculated in the local region. Considering two points A and B located at the interface of the local region which displacements

and rotations are known. Using a linear interpolation function it is possible to obtain in all the middle nodes between A and B of the CUF local model the displacements and rotations. Commercial codes only gives translational displacements (u_x, u_y, u_z) and rotations $(\theta_x, \theta_y, \theta_z)$ in the mid-plane in case of beams or plates. With the use of Lagrange polynomials in CUF it is needed to calculate the 3D displacements over the interface surfaces. In order to calculate the rest of nodes translations displacements Timoshenko can be applied for beams and Reissner - Mindlin for plates. As it is seen before, for 1D structures Timoshenko displacement field corresponds to:

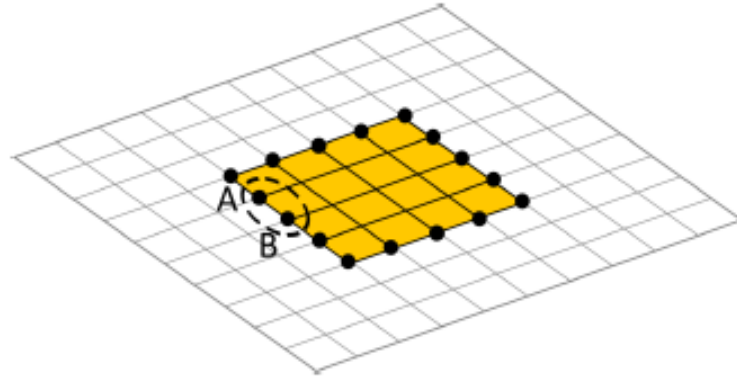
$$\begin{aligned}
u(x, y, z) &= u_0(y) \\
v(x, y, z) &= v_0(y) + x\phi_z(y) - z\phi_x(y) \\
w(x, y, z) &= w_0(y)
\end{aligned} \tag{5.1}$$

And when 2D plate structures have to be considered the Reissner - Mindlin displacement field is used:

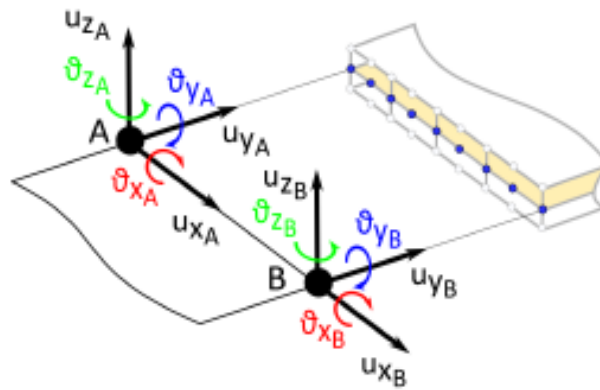
$$\begin{aligned}
u(x, y, z) &= u_0(x, y) + z\phi_y(x, y) \\
v(x, y, z) &= v_0(x, y) - z\phi_x(x, y) \\
w(x, y, z) &= w_0(x, y)
\end{aligned} \tag{5.2}$$

Where u_0, v_0, w_0 are the translational displacements and $\theta_x, \theta_y, \theta_z$ are the rotations of the global nodes located at the interface of the local region. In both cases, 1D or 2D, the rotations of the middle zone are used to compute the displacement of all the cross-section nodes at all the interface levels.

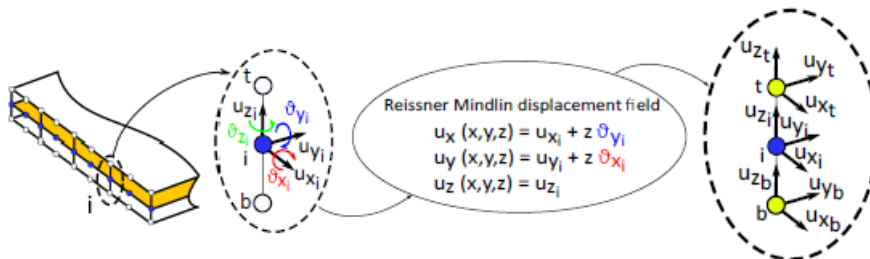
An example is shown in Fig.5.2(c). The displacements and rotations computed by the commercial code in the node i are used to find the displacements in the nodes t and b through the Reissner - Midlin displacement field.



(a) Arbitrary global and local region



(b) Global to local geometrical BC's



(c) Global and local kinematics

Figure 5.2: Global to local, *Source: [9]*.

5.2 Global local process and Python interface

To summarize the process that has been carried on in this thesis, displayed in Fig.5.3, is the following. First, the global model has to be designed and analysed using a (Nastran-FEMAP). Once the global model has been analysed, the local zone of interest has to be defined. The nodes that form this local zone are selected. To run the python interface two files from the Nastran are necessary. The bdf file containing all the information about the global model (this is the materials, the lamination, the mesh, the coordinate systems used etc) and a file

with the position, displacement and rotation of each node selected in the local zone. On the python interface the case of study and the local zone mesh are designed. Selecting the case of study is imposing which edges are free edges and which are continuous edges. In the free edges no boundary conditions will be imposed. In Fig.5.4 the local zone is shown. The local zone has to be defined by four straight lines forming four edges. So, 11 cases of study can be analysed, the case of four continuous edges, four cases with one free edge and six cases with two free edges. Regarding the mesh, the structural, the expansion mesh and their connectivities have to be defined. As they differ with beam or plate interface, the meshes are explained in the beam and plate interface sections.

Once the case of study has been selected and the mesh has been designed, the input files are written by the code. Finally the python interface offer the option to run the Mul2 analysis of the local zone created. In the appendix there are the manuals of the plate interface and the element wise interface (explained in the next sections).

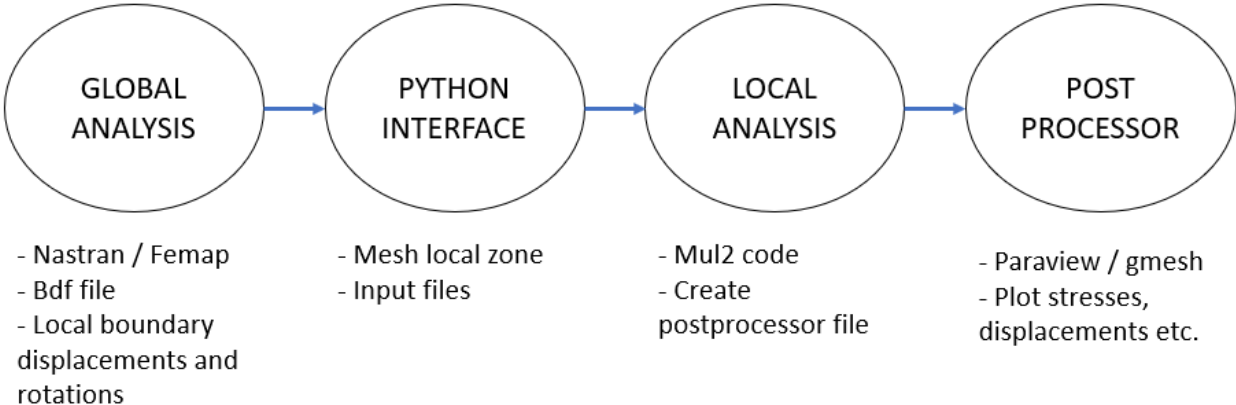


Figure 5.3: Global local analysis process

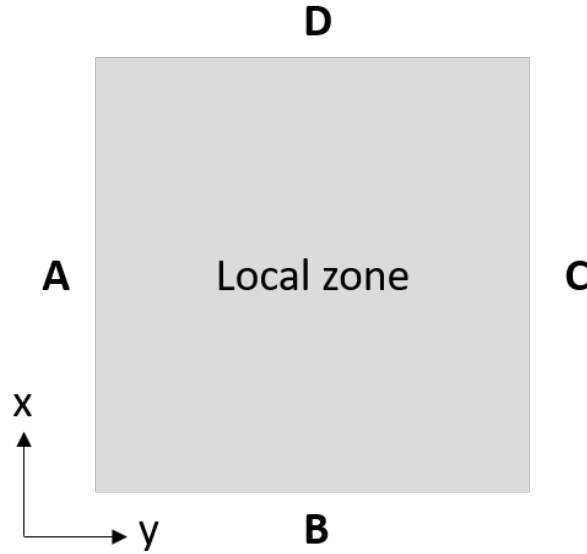


Figure 5.4: Local zone edges

5.2.1 Beam interface

The beam interface code was written before my incorporation on the project. In this code the local zone is always studied as a beam. Even if we have a very thin plate, the local zone mesh will be created with an expansion in the beam axis (y-axis).

So, the expansion mesh is created in the cross-section xz . This mesh can be designed with L9 elements or with L16 elements. This is the first choice that has to be done. Then, three different meshes can be selected. An equally spaced mesh, a chebysev mesh, or a square chebysev mesh. This two lasts meshes concentrate the nodes on the boundary resulting more reliable for the study of the free edge cases. Once the type of the mesh is selected, the number of elements in x and z have to be defined. The python interface will show a scheme with the mesh selected for the user and ask him if he is satisfied with the mesh. If not, the user will be able to redefine the mesh.

Regarding on the structural mesh, the number of elements B4 that are wanted for the structural direction (y) have to be defined.

Normally, the study of the different cases will include layers on the z direction. This layers can be composed by the same material changing only the orientation or by different materials. This last case was not considered in the original beam code and had to be implemented. Now, no matters how many materials compose the layers and how are this layers oriented the code is able to perform the analysis.

5.2.2 Plate interface

In order to carry out better analysis in 2D plates, the plate interface was implemented. This interface performs equally than the beam interface with the difference that i the structural mesh is defined in the xy plane and the expansion mesh is defined in the thickness direction (normally z direction). So, now, for the structural mesh Q9 or Q16 elements can be used and for the expansion mesh B4 elements are used. The code works similar to the beam code and it is explained in the manual that can be found in the appendix.

5.2.3 Element wise interface

The main limitation of the previous interfaces is that only work for a rectangular meshes like the local zone shown in Fig.5.4. But normally, in the structures that have to be analysed, specially in the aircrafts, the meshes are not regular and rectangular meshes. Instead of that the meshes are distorted like is shown in Fig.5.5.

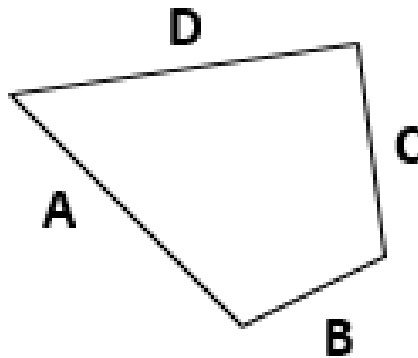


Figure 5.5: Distorted mesh

So, the last version of the code is working with an element wise (EW) interface. Four nodes composing an element have to be selected from the Nastran file. With the four nodes information (position, displacements and rotations) and the bdf file the analysis is launched. The code asks first if a free edge case wants to be considered or on contrary the four edges are continuous. Then the type of mesh that wants to be displayed (that is equidistant or chebysev mesh) is designed. If a free edge case is selected the next step is to indicate which of the four edges is the free edge. Then the number of elements (Q9 or Q16) along each edge have to be defined. Once the mesh has been decided and validated the input files will be create and the Mul2 code will be ready to launch the analysis of the local zone. In the manual in the appendix there is more details about the functioning of the code.

This code has no limitations in the orientation of the element in the space. There is no problem if the element is in the xy plane or xz plane or in a random plane. The code will extract the information of the element orientation and the material direction from the bdf.

5.2.4 The bdf file

The bdf file contains all the information referring the analysis model. This is, the different coordinate systems, the material and lamination data and the mesh designed, concretely the position of each node and the nodes that form each element as well as the coordinate system of the element. The property used in Nastran to define a laminate plate or beam is the PCOMP (PSHELL is used in absence of laminates). Inside this properties the different laminates are defined with the corresponding material and orientation. All this information is extracted in the Python code to be able to write all the input files presented in **Chapter 5**.

Chapter 6

Numerical results - Beam model

During this chapter the numerical results for beam models are presented. Two different beams are analysed. The first one, a cantilevered C section beam is analysed using a global CUF model through the Mul2 code. Then an eight layer beam is analysed first using a global CUF model and next using a global local model and the results obtained with both methods are compared.

6.1 Cantilivered C section beam

A cantilevered C-section beam is considered. The cross-section geometry is shown in Fig.6.1. The length-to-height ratio, L/h , is equal to 20. The height-to-thickness ratio, h/t , is as high as 10 with h and b_2 equal to 1 m, and b_1 as high as b_2 . Two point loads are applied at $[0, L, \pm 0.4]$. 6L9 distribution is adopted and shown in Fig.6.2. The material data is: the Young modulus, E , is equal to 75 GPa; the Poisson ratio, ν , is equal to 0.33. The model is analyzed through the Mul2 code entering the input files manually.

The analysis has been developed with 11349 DOF's, probably more than the necessities, but assuring more accuracy in the results.

The maximum vertical displacement, u_z , takes place at point $[-0.5, L, \pm 0.4]$ with a value of $-2.952 \cdot 10^{-8}$. The model is also analyzed with 9L9 distribution and the value calculated differs a bit from the previous one, been $-2.982 \cdot 10^{-8}$. This two values obtained by Lagrange expansion through the Mul2 code are compared with others values obtained from the Mul2 search group in [3] in Table 6.1. This models are the solid model that provides the exact solution but as it can be seen with a high computational cost (84600 DOF's), the Euler -

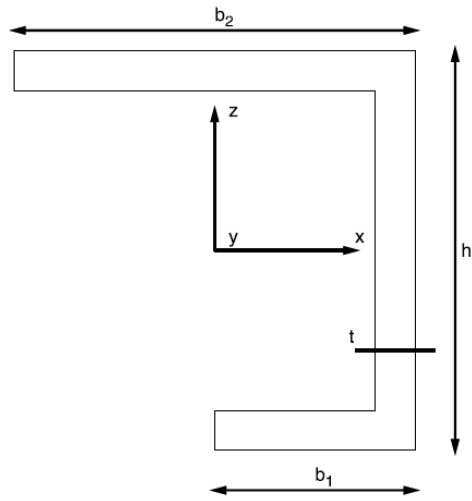


Figure 6.1: C section geometry.

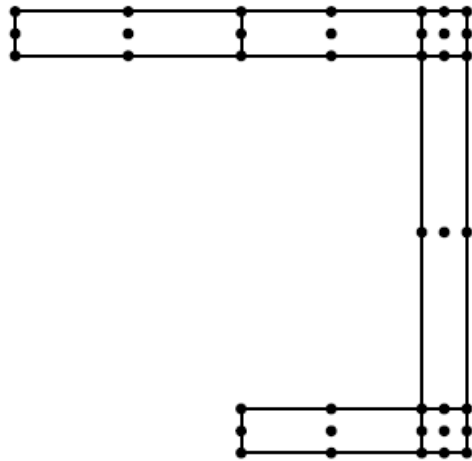


Figure 6.2: 6L9.

Bernoulli beam theory that is not able to detect the vertical displacement because of the hypothesis made by this model (see chapter 2) and different Taylor expansion models that with a higher order of expansion approximates the solution.

<i>model</i>	<i>DOFs</i>	$u_z \times 10^8$ [m]
SOLID	84600	-3.067
Taylor models [3]		
EBBM	155	0.0
N=4	1395	-0.245
N=8	4185	-2.161
N=11	7254	-2.565
LE models [3]		
6 L9	11349	-2.952
9 L9	5301	-2.982

Table 6.1: Degrees of freedom and maximum displacement for each model of the cantilevered C section beam.

6.2 Eight layer beam

A thick layer cantilever beam is considered. The beam is 90 mm long and its rectangular section is 10 mm high and 1 mm wide. Fig.6.3 shows the vertical distribution of the layers. Two different materials are employed for the lamination, 1 and 2. Both have the same elastic modulus in the transversal direction, E_T equal to 1 GPa, shear modulus, G_{TL} equal to 0.5 GPa, and poisson ratio, ν , equal to 0.25. The poisson ratio and the shear modulus are assumed to be constant in all directions. They differ in the longitudinal elastic modulus, wich is 30 GPa for material 1 and 5 GPa for material 2. Four equal loads are applied at the corners of the beam's tip, summing a total of -0.2 N in the vertical direction.

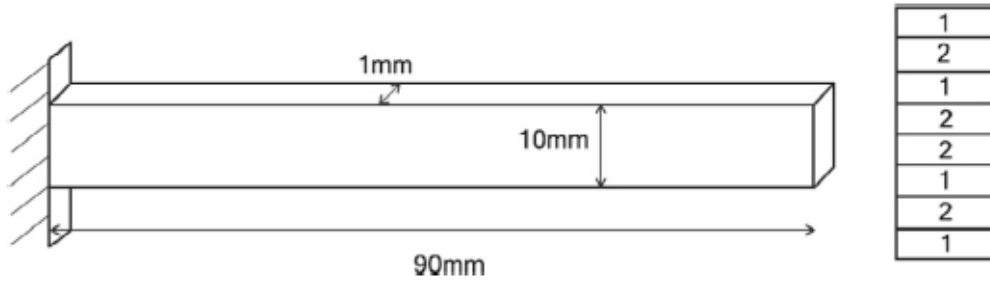


Figure 6.3: C section geometry.

6.2.1 Global model

The eighth layer beam is analyzed using the CUF formulation and the Mul2 code. 8L9 elements are used in the x-z plane, one for each layer. The input data is entered manually and the results are analyzed with Paraview. Fig.6.4 shows the deformed beam and the displacements along z axis. The maximum u_z occurs in the free end of the beam with a value of $3.01 \cdot 10^{-5}$.

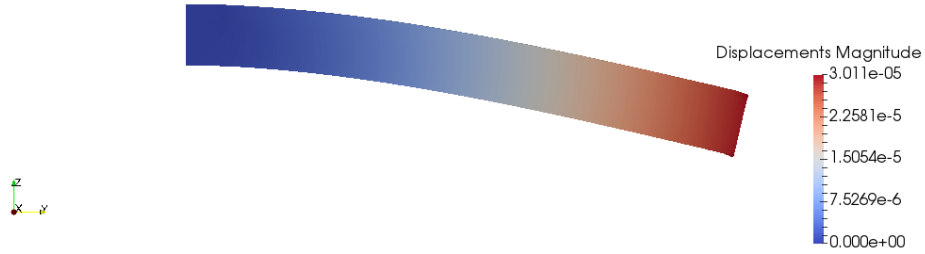


Figure 6.4: Displacements of the eight-layer beam

The stresses at the mid span along the z axis of the beam can also be analyzed with Paraview. σ_{yy} and σ_{yz} at mid span are shown at Fig.6.5.

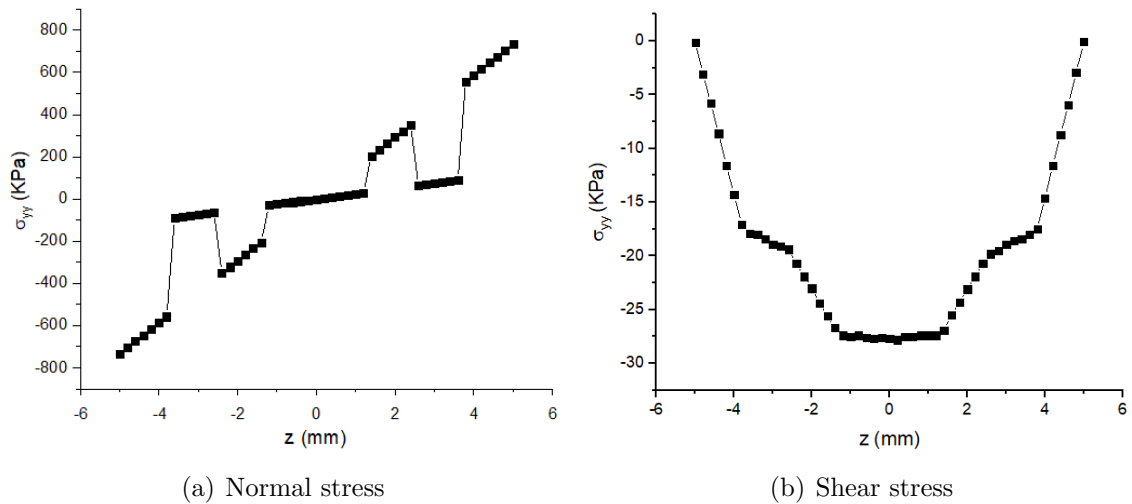


Figure 6.5: Normal and shear stress distribution along the z-axis at mid-span for the eight-layer beam.

6.2.2 Global local model

The same beam is analyzed using a global local model. The global model is designed with FEMAP with the laminate plate property. The mesh used and the translation along z axis is shown at Fig.6.6. The maximum displacement along z axis, $3.04 \cdot 10^{-5}$, that occurs in the free edge differs a bit from the value obtained with the CUF formulation.

Once we have the global model, we can perform local analysis using the interface code developed with Python. From the global model and the displacements at the boundary of the zone of interest the code will create the input files that will be entered in the Mul2 code.

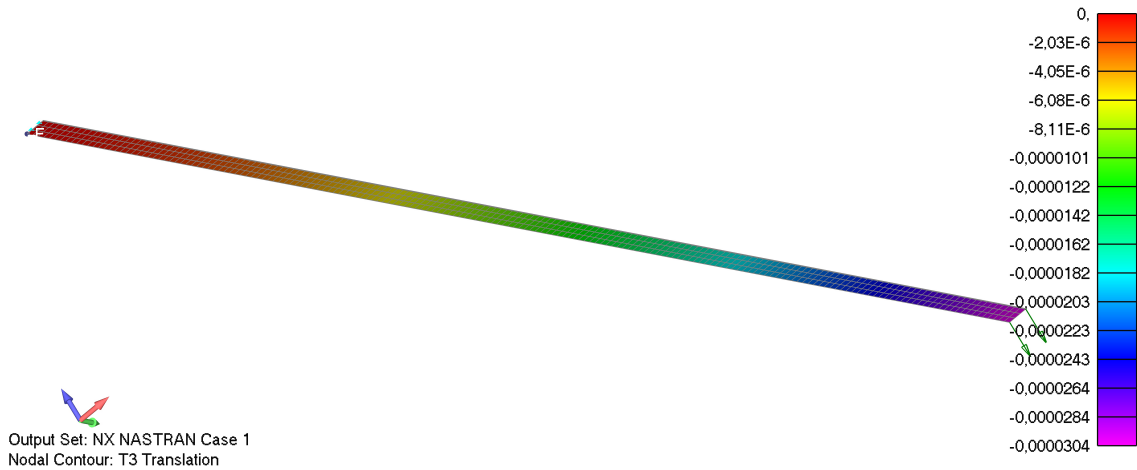


Figure 6.6: 2D eighth layer beam z displacements.

At the python interface the case of study (il est the sides of the zone of interest where we applied boundary conditions),the type of mesh and the number of divisions along each axis have to be indicated. The python interface code has been adapted to be able to launch the analysis with layers composed with different materials. The code was only able to discern between layers with different orientation.

Once the Mul2 code is launched with the condicions named before, postprocessor analysis is performed with Paraview. Stresses at mid span can be analyzed and compared with those found with the global model. A local zone in the mid span of the beam is considered. The stresses at mid span are represented at Fig.6.7 as well as those stresses calculated by the global model. It can be observed that both models detect perfectly the stresses.

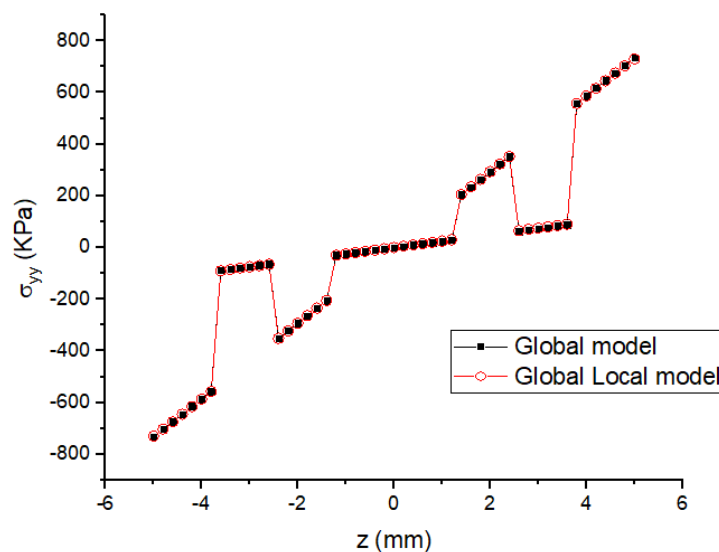


Figure 6.7: Normal stress distribution along the z-axis at mid span

Layers with different orientation

In order to validate the code modification a more complex example is considered. The same beam with the eighth layers is considered. The material composition of the layers is not changed but now different orientations of the layers are imposed. From the top to bottom the angles of the layers are $[0, 90, 45, -45, -45, 45, 90, 0]$ ($^\circ$) and the materials are still $[1, 2, 1, 2, 2, 1, 2, 1]$. So now, instead of two different layers, four different layers are considered and shown at table.6.2.

Layer	Material	Angle
1	1	0
2	2	90
3	2	-45
4	1	45

Table 6.2: Eight layer beam lamination.

Using the same group created for the previous example stresses at mid span are shown at Fig.6.8. Normal stresses varies from those obtained before. Logically stresses at the first and last layers are the same as this layers are oriented equally as before. Basically the stresses at the third and fifth layers varies from 50000 Pa to almost 0. In the Fig.6.8 also stresses calculated by Nastran are shown.

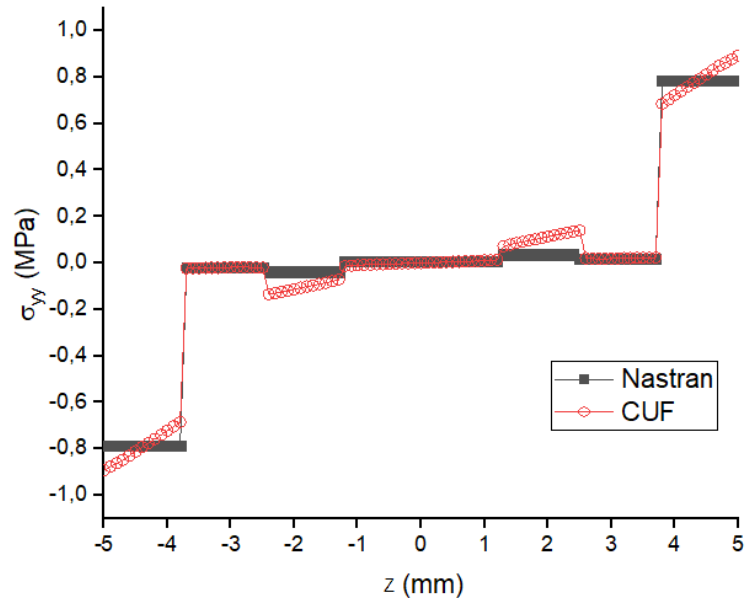


Figure 6.8: Normal stress distribution along the z-axis at mid span

Chapter 7

Numerical Results - Plate Model

The Numerical results for different plate model are presented in this chapter. Three different models are analysed. First a 3 ply composite rectangular plate under bending is studied using a CUF global local model and the results obtained with this method are compared with those obtained by Nastran. Then to carry out an EW approach with an irregular mesh approach a plate hole model is analysed. Finally a part of an aircraft wing provided by Embraer SA is studied both with the plate interface and the EW approach.

7.1 3 Ply Composite Rectangular Plate Under Bending

A 3 plies composite plate is considered. The plate is free at one end and clamped at the other end. The cross-section is shown in Fig.7.1. At the centre of the free end the structure is loaded by a point load in z-direction its magnitude is $-1 \cdot 10^{-3}$. The plate dimensions are $L = 2.0$ m (length) and $b = 0.1$ m (width). Each ply has a thickness of $t_{ply} = 0.001$ m resulting to a total thickness of the plate of $t = 0.003$ m. The stacking sequence of the laminate is $[0, 90, 0]$ ($^{\circ}$). The material considered for the plate is an orthotropic material with the following properties: $E_{11} = 40$ GPa, $E_{22} = E_{33} = 4.0$ GPa, $\nu_{12} = \nu_{13} = \nu_{23} = 0.25$, $G_{12} = G_{13} = G_{23} = 1.0$ GPa. The Global model is realized in MSc-Nastran with Femap and a mesh of 10×200 plate elements is considered. The local region taken into account constitutes a small region within the global structure. The local region is located at the central of the model and its geometrical parameters are the followings: $L_{local} = 10.0$ mm, $b_{local} = 10.0$ mm and the thickness of the plate $h_{local} = t = 3.0$ mm. In the Fig.7.2 the global structure is shown with the local region selected for the analysis.

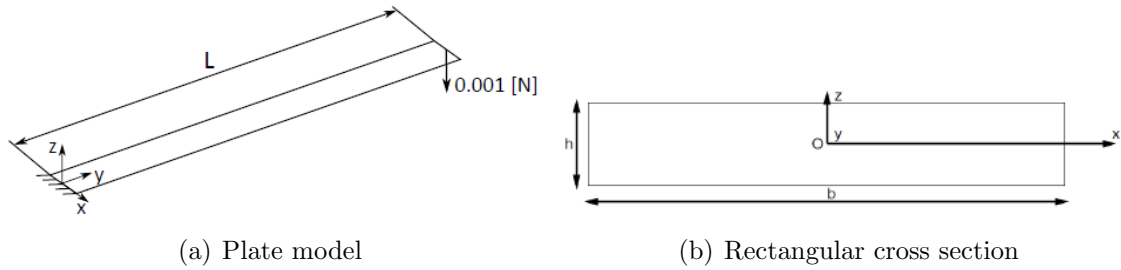


Figure 7.1: Plate model and geometrical features

This example was before analysed considering the plate a beam with the cross-section in the plane x - z . The CUF local model considered was 20 B4 structural elements used along the y -axis direction and then the LE (Lagrange Expansion) sub-domain distribution along the plane x - z . Two different sub-domain distributions were adopted. The first one consists of 5×9 L9 sub-domains (5 along x and 9 along z) while the second one consists of 5×9 L16 sub-domains (5 along x and 9 along z) with 3 sub-domains for each layer of the structure. The results are in the report [9]. With the development of a python interface suitable to work with plates the same problem is carried on but in this case the CUF model considered varies. The expansion mesh takes place in the z axis with 3 B4 structural elements (one for each layer) and the structural mesh is defined in the x - y plane. The sub-domain adopted was 10×10 L9.

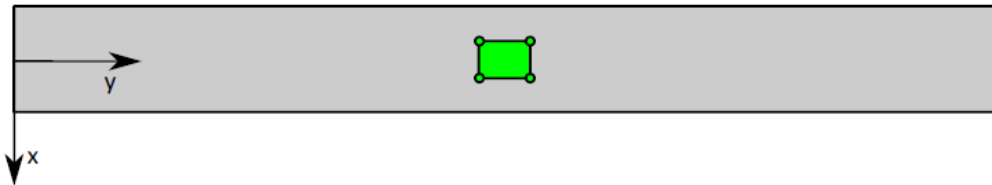
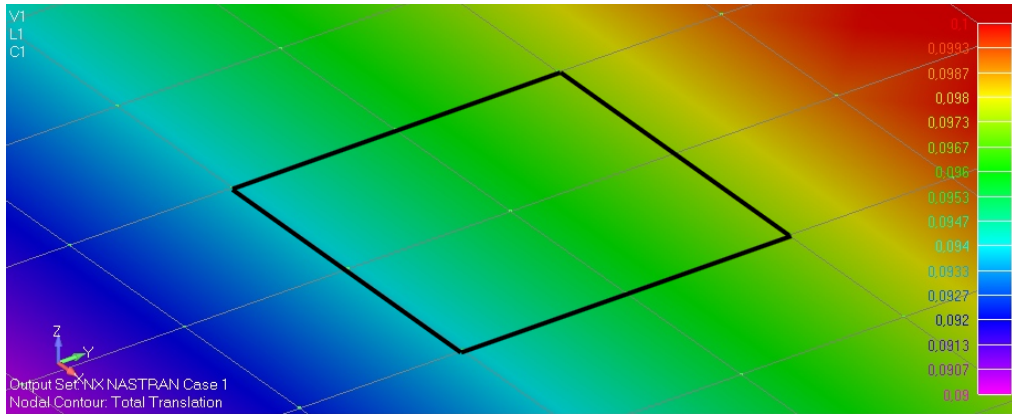
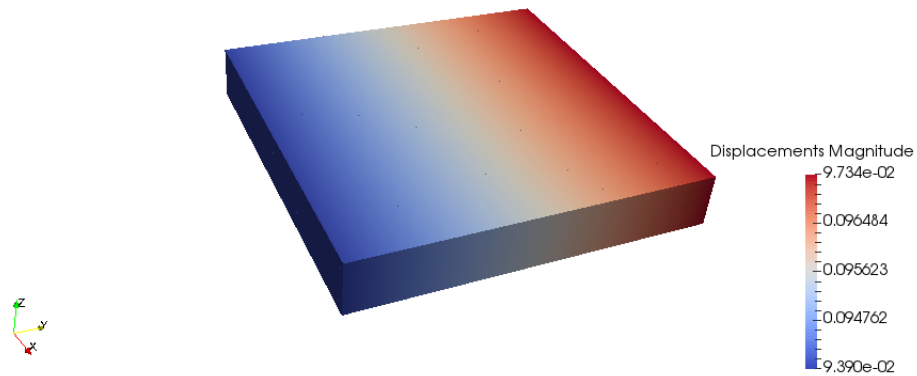


Figure 7.2: Local region

In Fig.7.3 the comparison between the global displacements calculated by Nastran and the local displacements obtained by the CUF formulation through the Mul2 code is displayed. As it can be observed, the displacements obtained by the two different ways are the same with a values between 0,09390 and 0,09734 mm.



(a) Displacements on the mid span local zone obtained by Nastran



(b) Displacements on the mid span local zone obtained by CUF (Mul2 code)

Figure 7.3: Local zone displacements

Regarding on the stresses, σ_{yy} and σ_{yz} are studied. The comparison between the stresses obtained by Nastran and by CUF is displayed in Fig.7.4. It can be observed that in Nastran code always give a constant value on each layer of in-plane or out-plane stresses. With the global/local approach, it is possible to predict the behaviour of all the stresses. The results of the Nastran code coincide with the global/local model only in the middle of each layer. Also, the global/local model capture the quadratic behaviour of the shear stress.

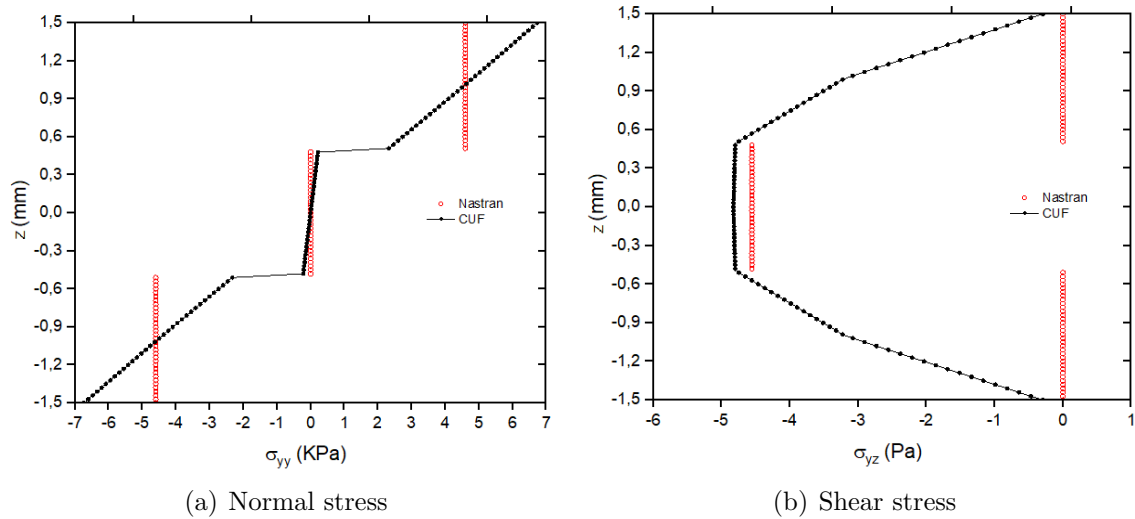


Figure 7.4: Normal and shear stress distribution along the z-axis at mid span

7.2 Plate hole: the element wise approach

The next example analysed is the typical plate hole under a pressure load applied on the two sides of the plate. This case is not a composite laminate problem but is useful to validate the element wise Python code. With the previous codes (beam and plate interface) was not possible to analyse irregular meshes so an element wise code had to be programmed in order to be able to perform this type of analysis. As the name indicates this code takes only one element of the mesh and create the input files for the Mul2 code of this element as it was explained before.

In the Fig.7.5 the geometrical features of the plate are shown.

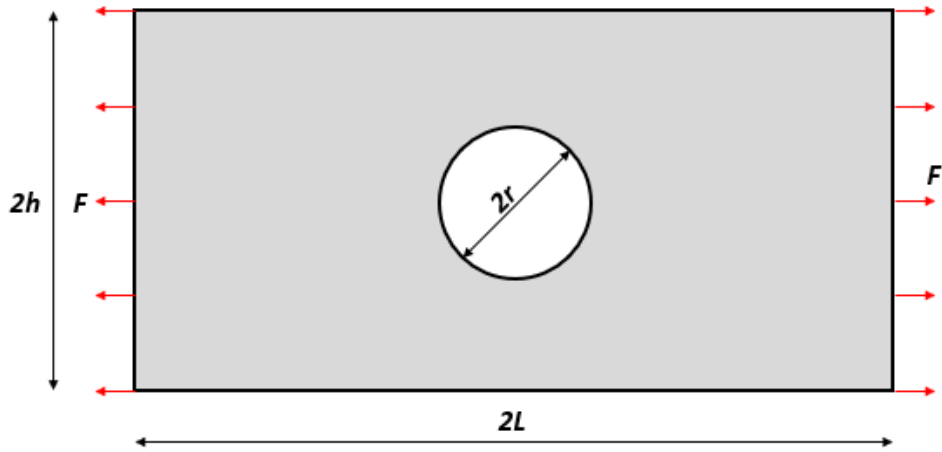


Figure 7.5: Plate hole model and geometrical features

The dimensions of the plate are $L = 100$ mm and $h = 50$ mm and a hole of radius $r = 20$ mm. The material considered is steel with properties of Young's Modulus $E = 210000$ MPa and Poisson's ratio $\nu = 0.3$. The pressure load considered for this problem has a value of $F = 100$ N/mm².

The plate has no boundary conditions, so it is not fixed in space. This introduces a degree of freedom that is not wanted in finite element analysis. To solve that, symmetries are used. The symmetries will play the role of boundary conditions and moreover will reduce the number of elements in the analysis. So, the problem is reduced to the structure shown in Fig. 7.6.

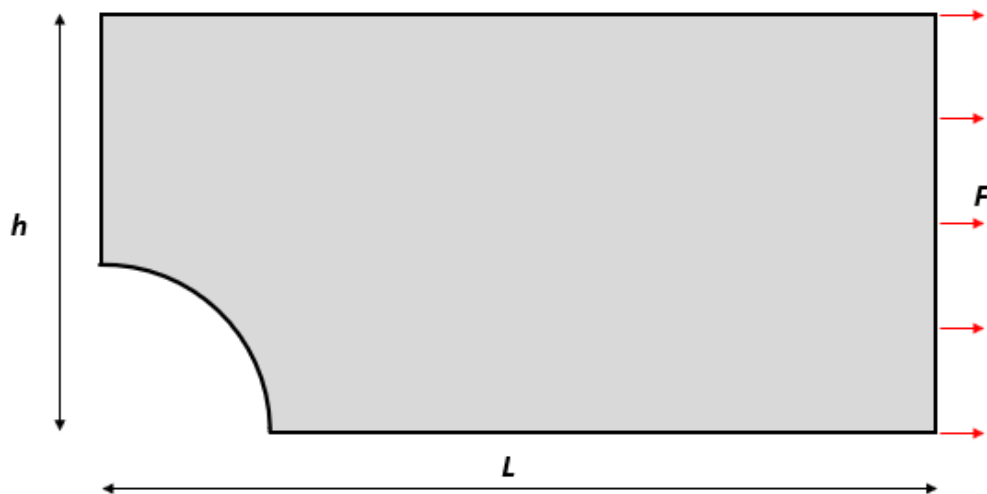


Figure 7.6: Plate hole reduced model

The problem is solved with Femap (Nastran). The mesh structure is shown in Fig. 7.7. The mesh is rectangular with the exception of the elements around the arc which are irregular.

This zone will be the critical one.

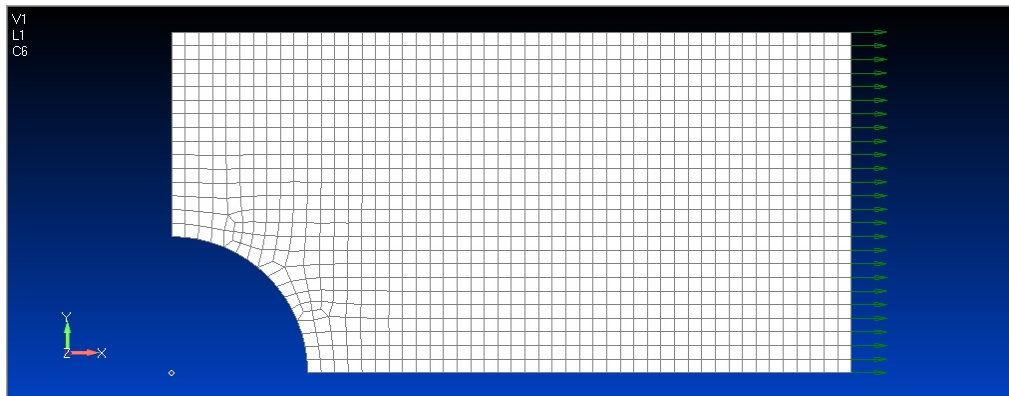


Figure 7.7: Plate hole mesh structure

In Fig.7.8 and Fig.7.9 total displacements and Von Misses stresses are displayed. The most critical element of the structure is marked with a black arrow.

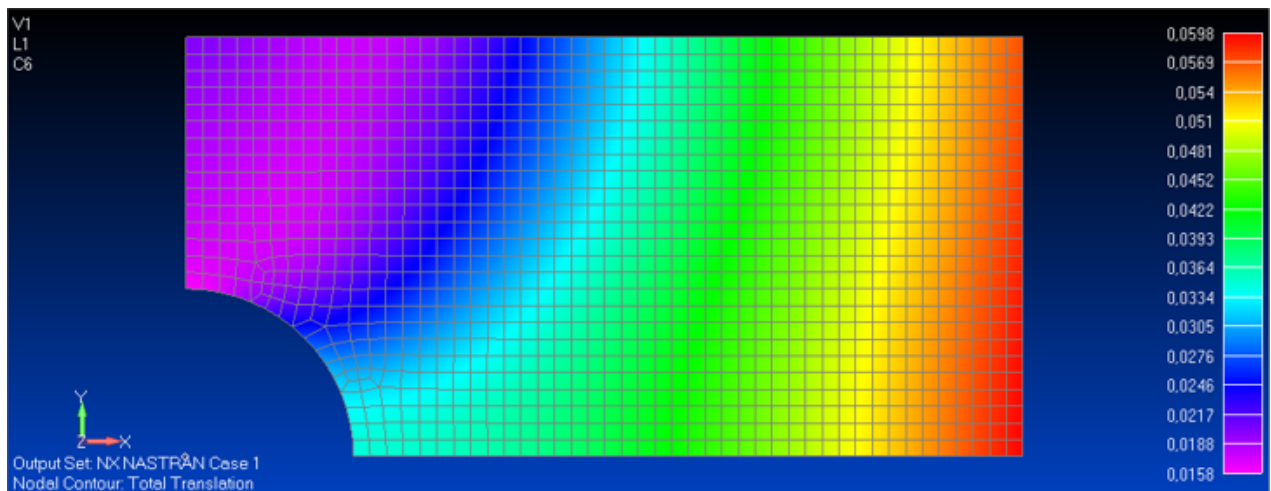


Figure 7.8: Plate hole global total translation

In this case the results have credibility as the plate is made from an isotropic material and without composite laminates. But it is an interesting example in order to validate the python element wise interface, for example checking the displacement results inside the element and comparing those results with the Nastran results. In Fig.7.10 the displacements in the critical element of the structure are shown and correspond with the Nastran displacements shown in Fig.7.8.

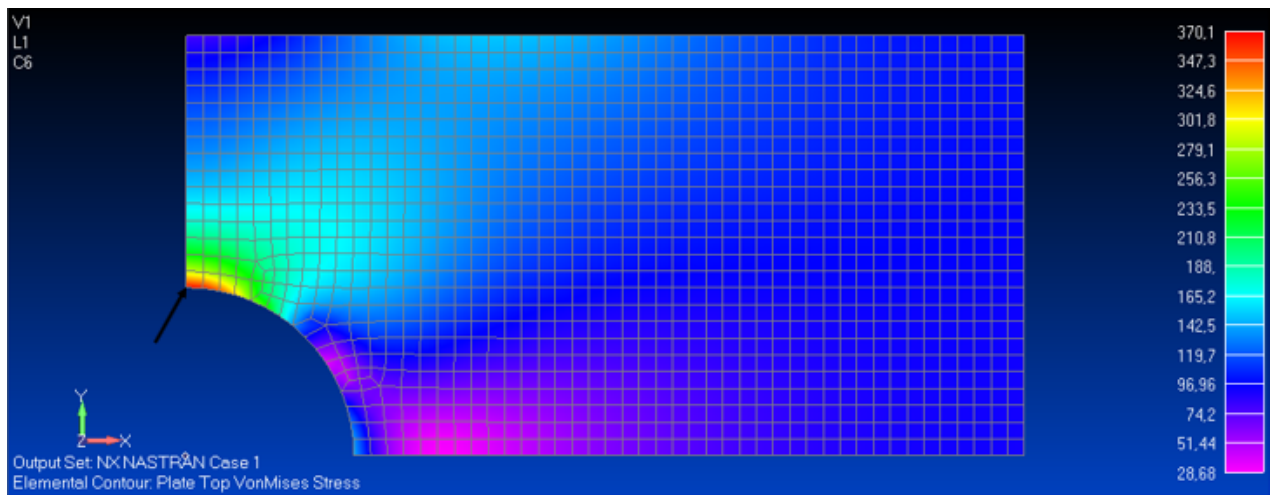


Figure 7.9: Plate hole Von Misses stresses

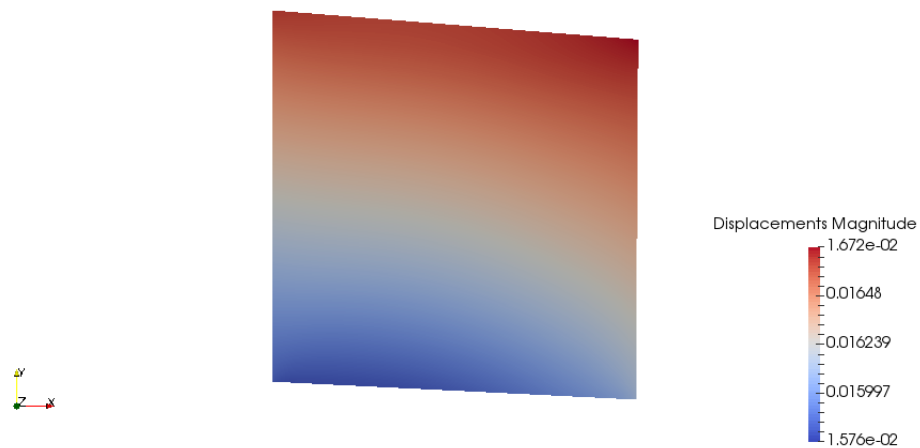


Figure 7.10: Plate hole displacements in the most critical element

With the global/local analysis is possible to plot the displacements in the thickness direction (z axis). This displacements are displayed in Fig.7.11.

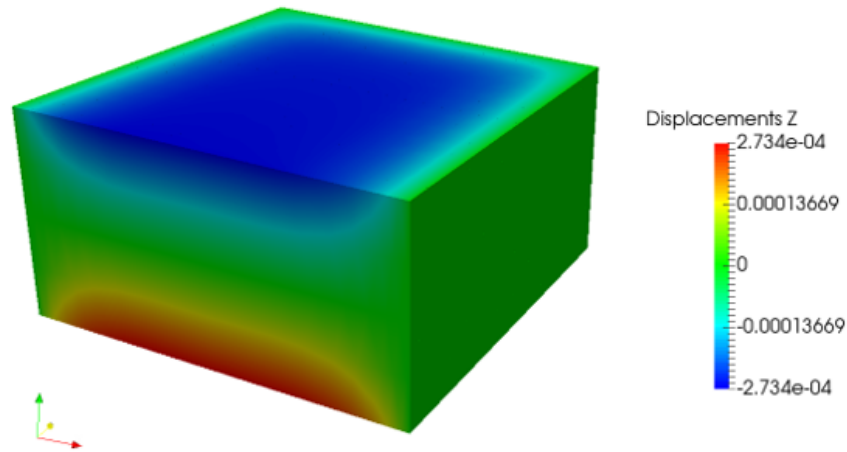


Figure 7.11: Plate hole displacements in z direction of the most critical element

Finally the Von Mises stresses in the element analyzed are shown in Fig.7.12. As it can be observed those stresses correspond with the stresses calculated by Nastran.

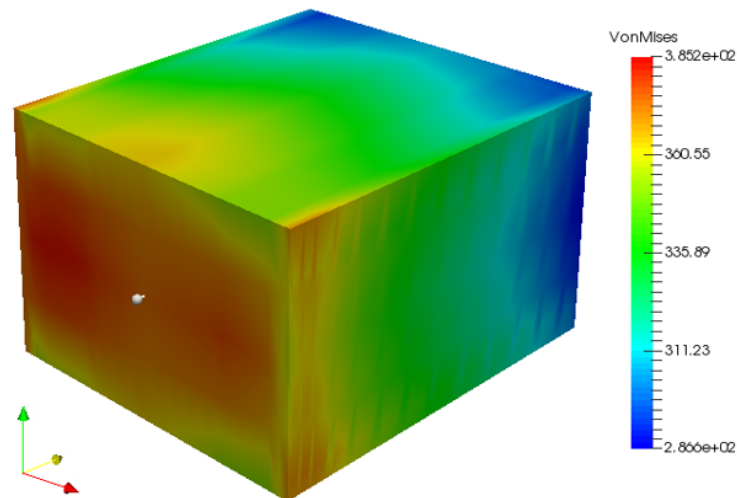


Figure 7.12: Plate hole Von Mises stresses in the most critical element

7.3 Wing structure

A part of a wing structure is analysed. This example has been provided by Embraer SA, company that collaborates with PoliTO in different projects. The structure is displayed in Fig.7.13. The hole was not in the original wing structure but in order to make the wing a more academic example the hole has been introduced. The part has a length of 0.6 m, a width of 0.8 m and a height of 0,05 m. The wing structure is fixed on three sides as it can be seen in Fig.7.13. The fourth side is under a punctual compressive force that acts on the centre

of the y-axis ($y = 0.4 \text{ m}$) and on $z = 0.02 \text{ m}$ with a value of 500000 N .

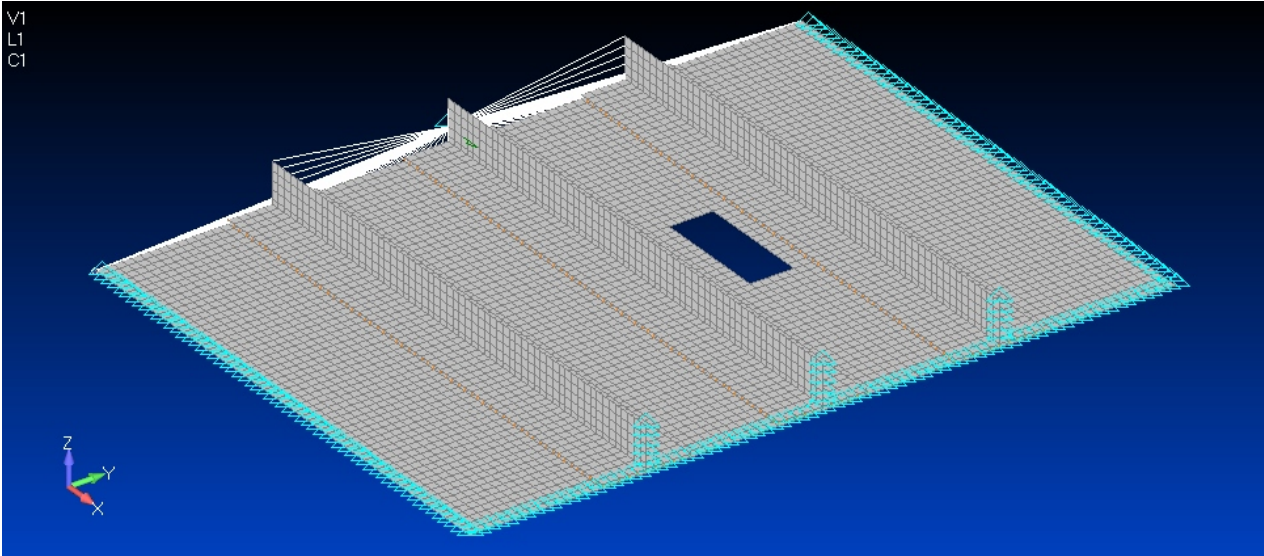


Figure 7.13: Wing model and constraints

The wing is made from an orthotropic material and composed by 12 laminates. The material properties are the following: $E_{11} = 165 \text{ GPa}$, $E_{22} = E_{33} = 9.0 \text{ GPa}$, $\nu_{12} = \nu_{13} = \nu_{23} = 0.34$, $G_{12} = G_{13} = 5.6 \text{ GPa}$ and $G_{23} = 2.8 \text{ GPa}$. The stack sequence is $[0, 90, 45, -45, 0, 0, 0, 0, -45, 45, 90, 0]^\circ$.

As it is said before when it comes to composite laminates the results given by Nastran are not totally reliable in the critical zones. But they can give a first approach, an approximation of the real solution and detect which zones are the most critical in order to then work on the local approach in these zones. That occurs specially for the stresses and not for the displacements. In Fig.7.14 the displacements of the model are displayed.

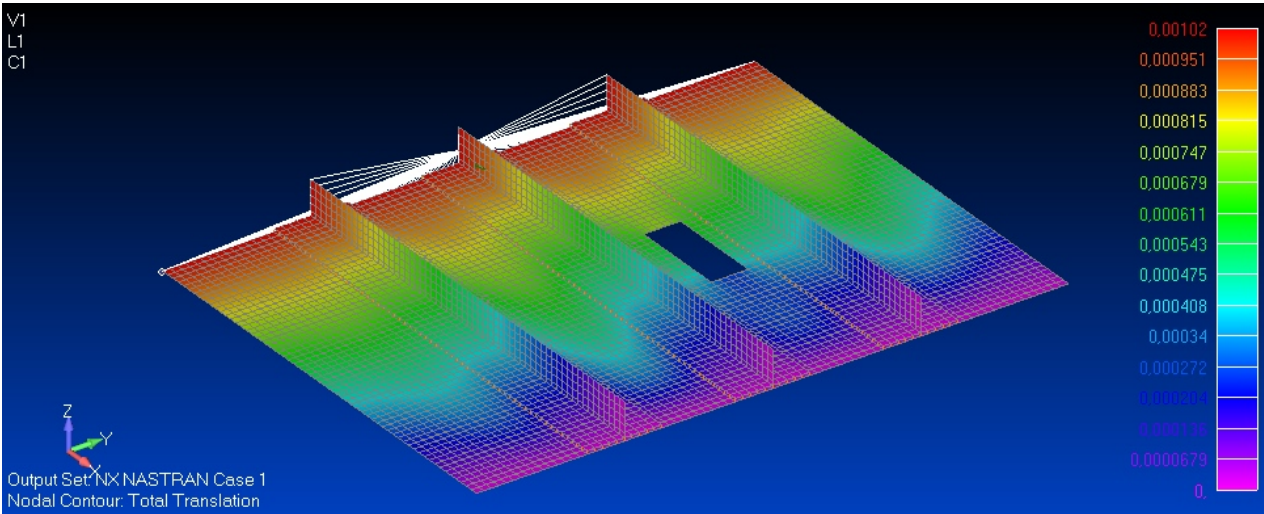


Figure 7.14: Wing structure displacements

σ_{xx} stresses are studied in the first layer in order to find where are the critical zones of the wing structure. σ_{xx} stresses are displayed in Fig.7.15. Logically the most critical part of the structure is the zones around the hole where the stresses achieve the maximum. In order to do an exhaustive analysis all the components of the stresses of all of the layers would have to be analysed, but an academic analysis is been performed to be able to validate the code programmed. In Fig.7.16 a zoom in the zone around the hole is displayed.

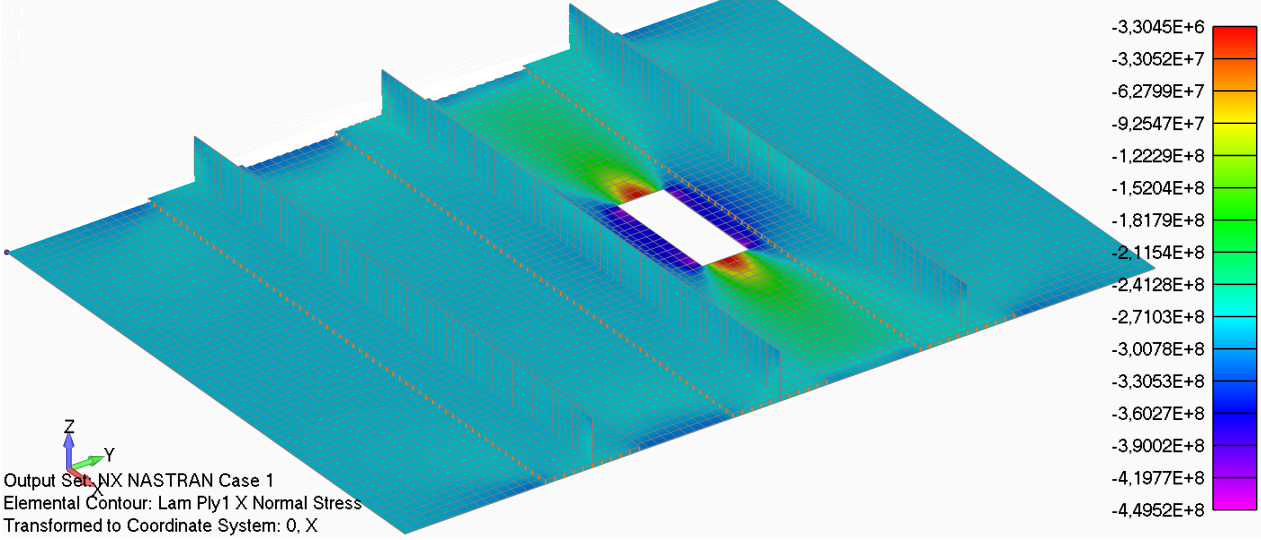


Figure 7.15: Wing structure σ_{xx} stresses at the first layer

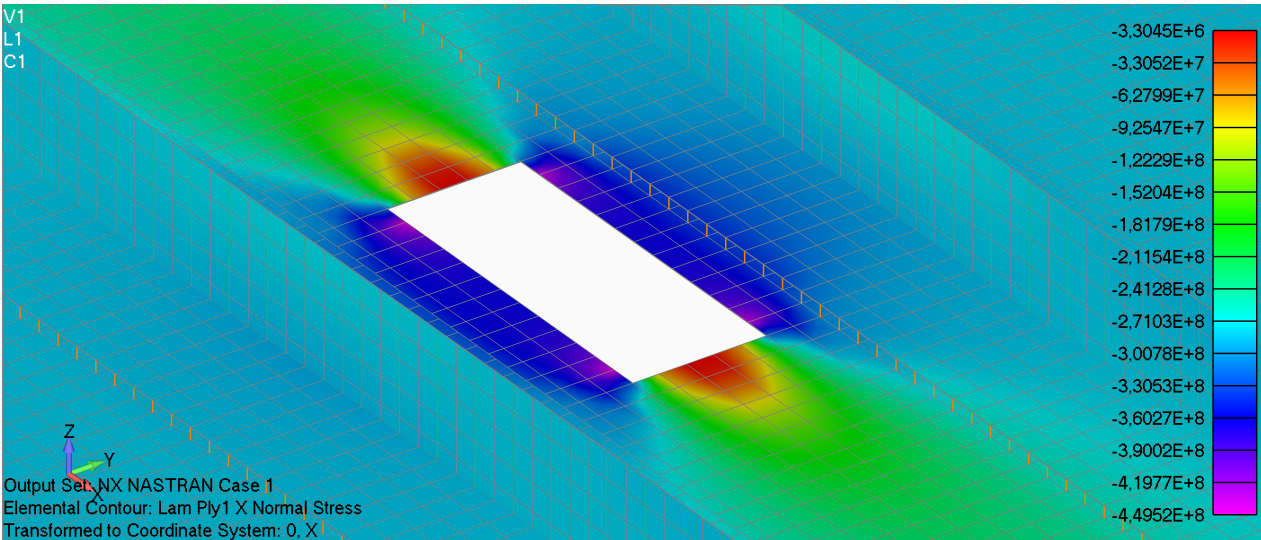


Figure 7.16: Wing structure σ_{xx} stresses around the hole

Accounting this the wing will be first analysed around the hole using the python plate interface and analysing the free edge effect with both the plate interface and the element wise interface. Then, an element wise analysis on the vertical surface is also been carried on in

order to validate that the code is able to work no matters the orientation of the element that is been studied.

7.3.1 Local analysis around the hole

The four sides of the hole are been analysed. This is done for validate that the code is able to study the four cases of free edge that are presented in this problem. Looking at Fig.5.4 the edges A and C are those that have a constant y coordinate and the edges B and D those with x coordinate constant. The four local zones are highlighted in Fig.7.17 with the free edge marked with the corresponding letter in white.

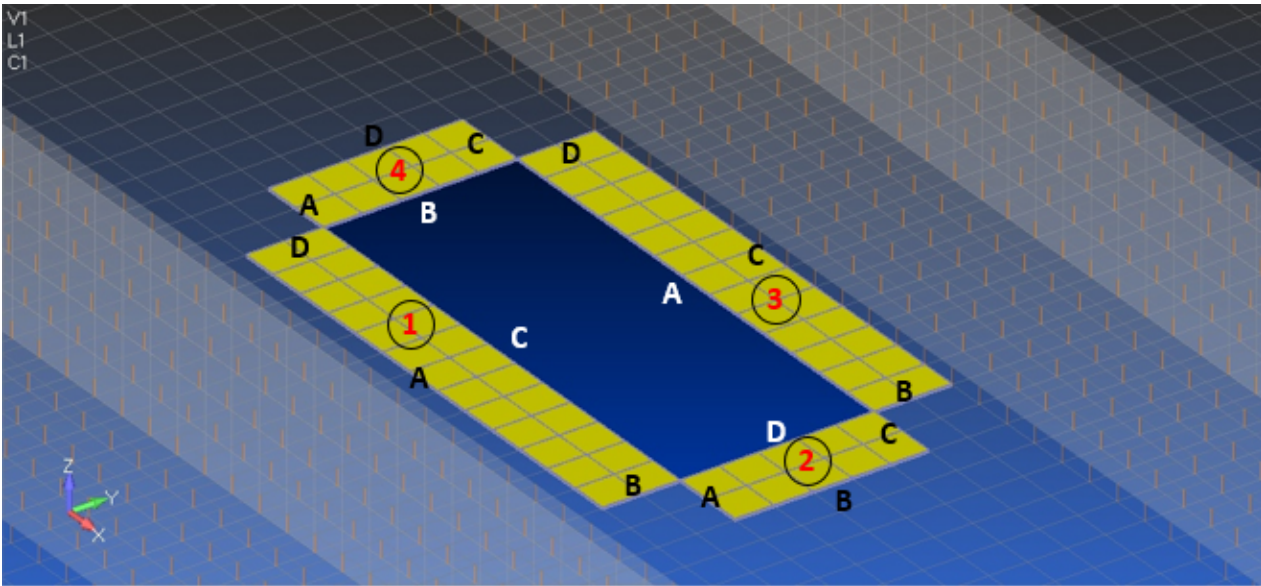


Figure 7.17: Local zones to be studied

The CUF local analysis is been carried out with $4L9 \times 8L9$ elements in plane in the local zones 2 and 4 and $10L9 \times 4L9$ in the 1 and 3 local zones. Regarding on the elements per layer, two B4 elements per layer have been used for all four local zones. As these are cases with a free edge chebysev distribution of the nodes has been used in order to obtain better results. The first thing to validate in each zone is the displacements. In Fig.7.18 the displacements around the hole calculated by Nastran are shown. This displacements are compared with those resulting of the local analysis displayed in Fig.7.19. As it can be observed the displacements calculated with the global model and the local model are the same as it is expected.

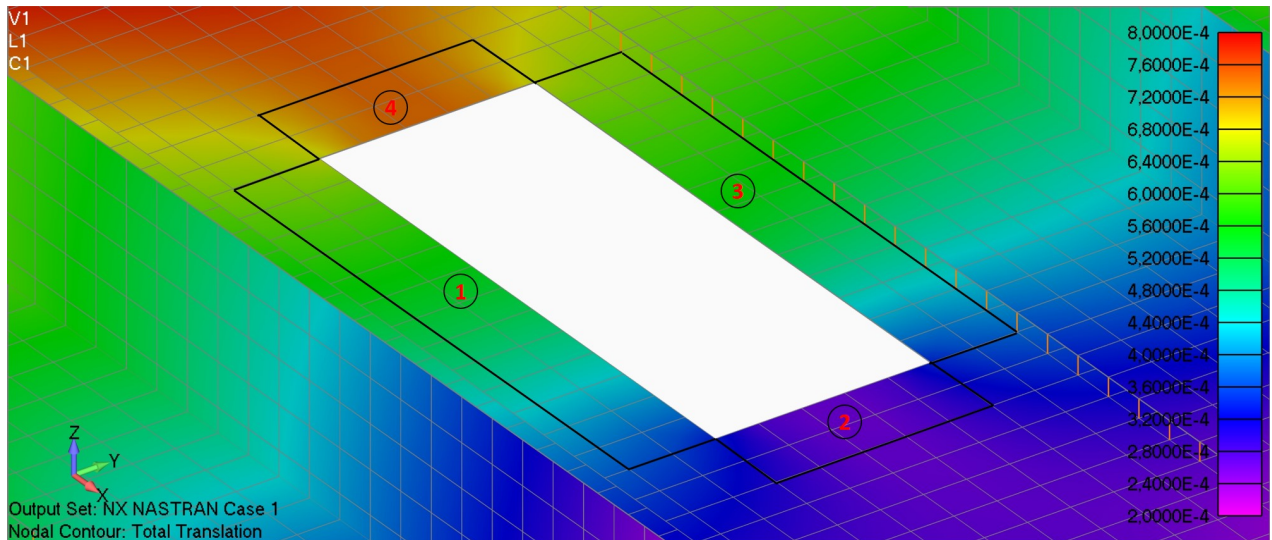


Figure 7.18: Total displacements around the hole

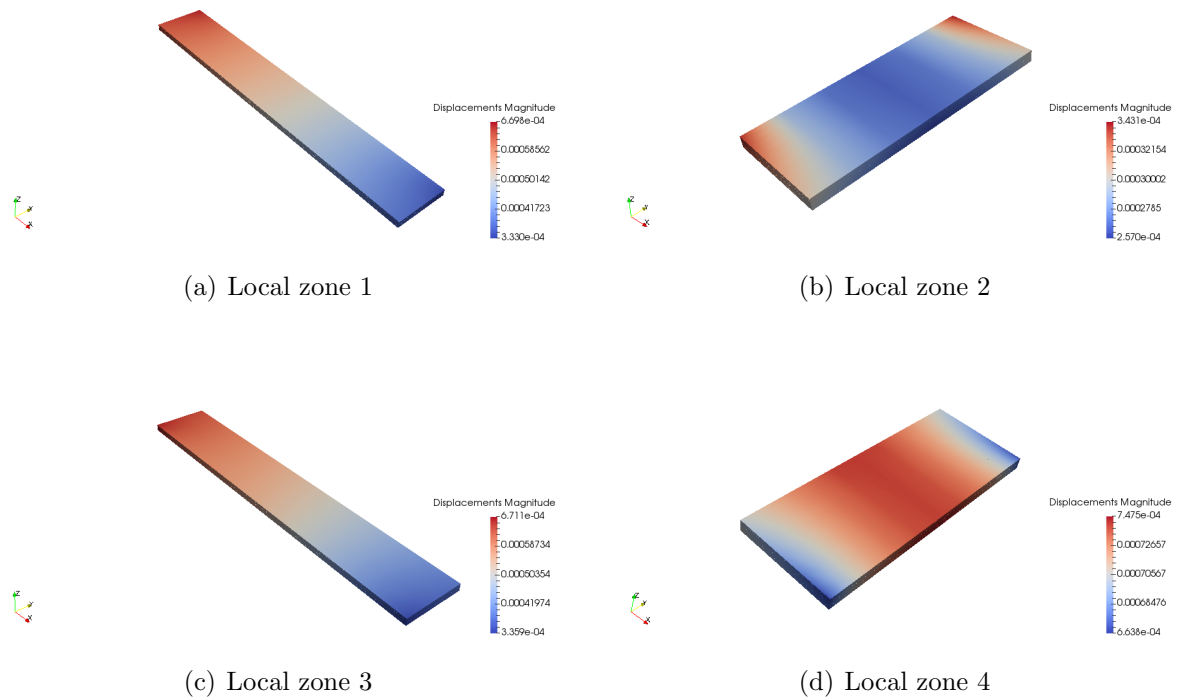


Figure 7.19: CUF local zone displacements

Once the displacements are validated the analysis of the stresses are performed. The stresses taken into account are the stresses in plane, σ_{xx} , σ_{yy} and σ_{xy} and the stresses out of plane, σ_{yz} and σ_{xz} . The point analysed in local zone 1 is located at the centre of x coordinate and near the free edge, is the point A of the Fig.7.20.

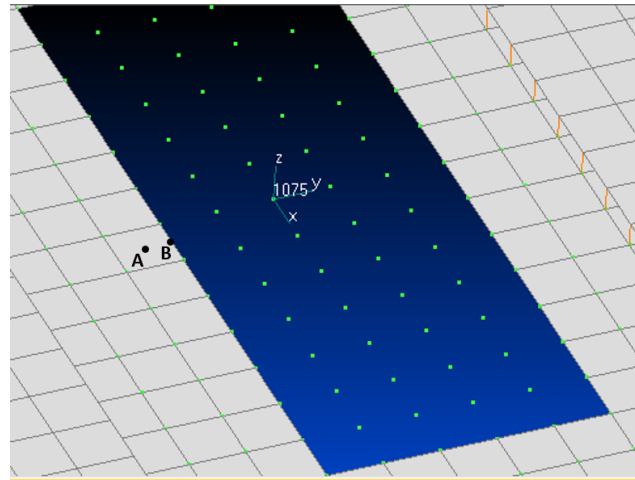
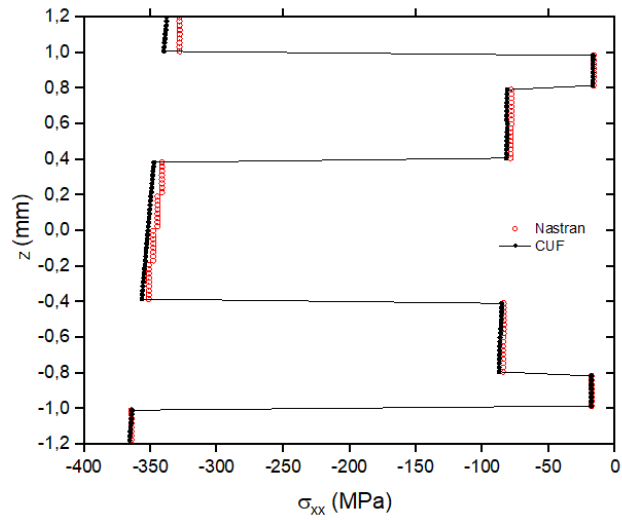
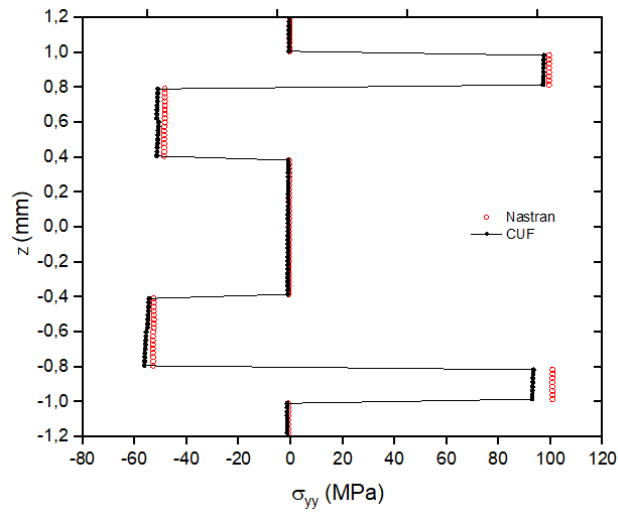


Figure 7.20: Points where the analysis have been developed.

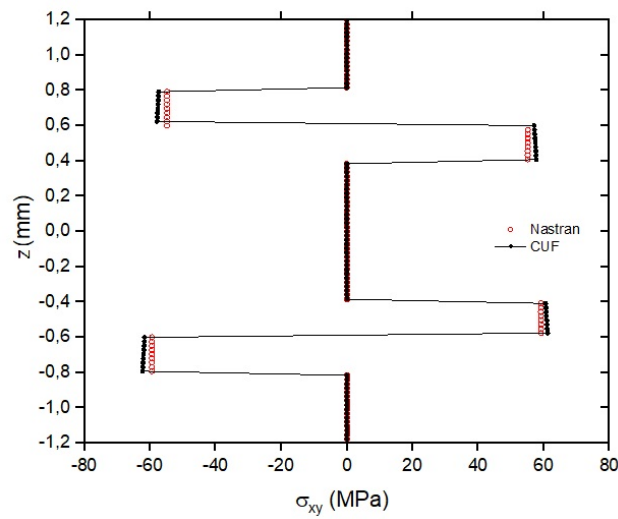
In Fig.7.21 the stresses in plane are represented. All the graphs show the stresses calculated by Nastran and by the CUF.



(a) Normal stress - σ_{xx}



(b) Normal stress - σ_{yy}



(c) Shear stress - σ_{xy}

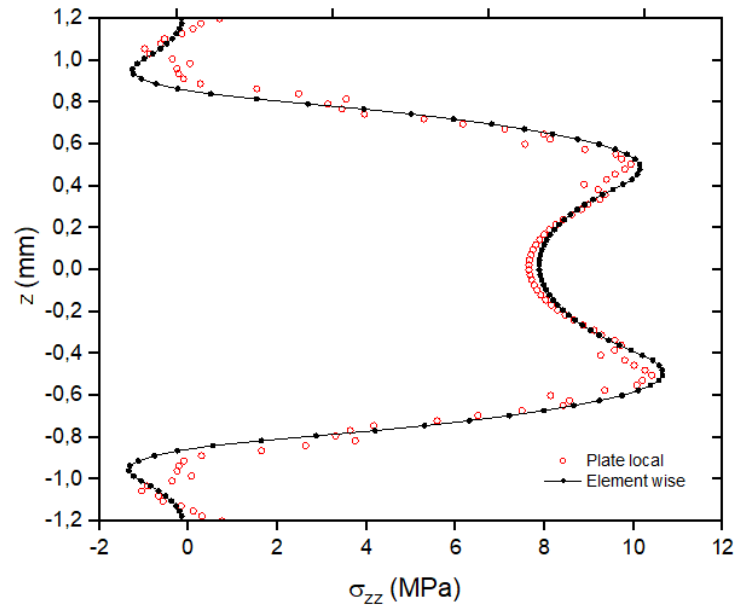
Figure 7.21: Normal and shear stresses in plane

It can be observed that Nastran is able to approximate well the stresses in plane but it shows always a constant value along each layer on contrast with the CUF model that is able to plot the exact value in every point of the layer.

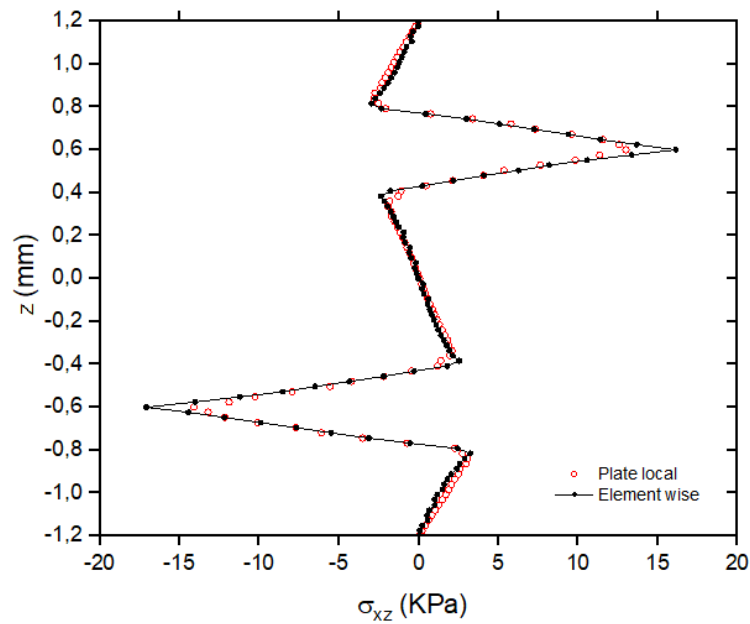
Free edge analysis

In the free edges of a composite laminates high and interlaminar stresses are present. This stresses are consequence of the mismatch in elastic properties between plies and can cause edge delamination or interlaminar fracture in the composites laminates that are manufactured by conventional lay-up technique. This delamination might lead to severe safety problems, for example the reduction of stiffens, strength and fatigue life. Therefore, is important to understand the behaviour of this stresses in order to prevent the failure of the composite laminate at free edges.

A free edge analysis is performed in point B of the Fig.7.20. The stresses taken into account in this analysis are σ_{zz} and σ_{xz} . The stresses at this point are analysed using the local model introduced before and doing an element wise analysis in the element where the point is located. This analysis has been carried on with 8Q9 elements per each side of the element and 2B4 elements per layer. The structural mesh has been meshed with a chebysev model. In Fig.7.22 there is the comparison of the values of σ_{zz} and σ_{xz} obtained by the plate local model and the element wise model.



(a) Normal stress - σ_{zz}



(b) Shear stress - σ_{yz}

Figure 7.22: Normal and shear stresses out plane in the free-edge

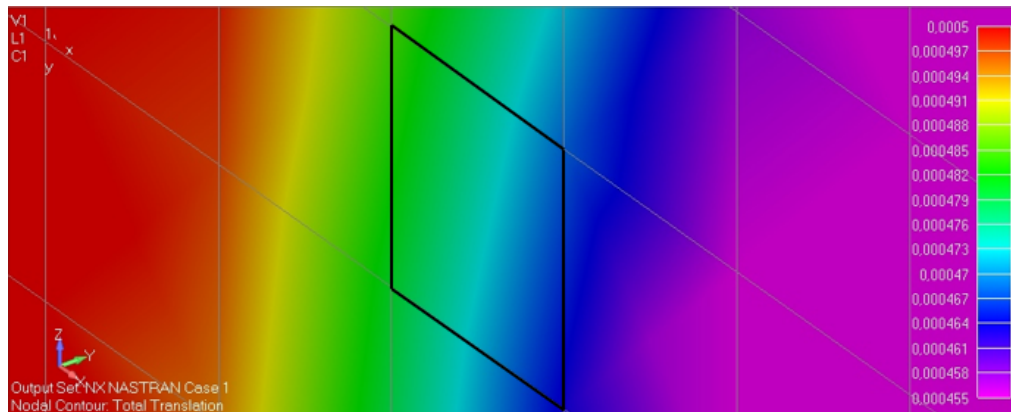
It can be observed that both models, the plate local model that contains the zone 1 of the Fig.5.4 and the element model that only constitute the element that contains point A and B and that is a more refined model, obtain approximative the same values of the stresses out-plane in the free-edge on contrary that Nastran that is not able to obtain this stresses out-plane in the free-edge in case of composites.

7.3.2 Element wise analysis

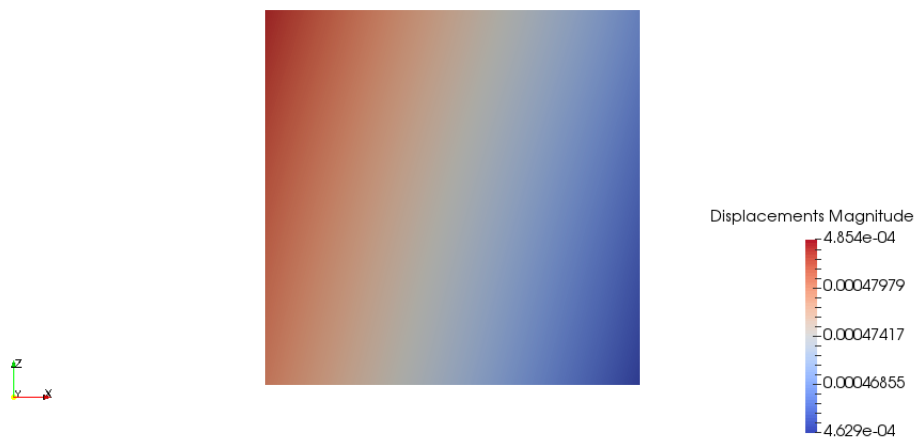
A random element placed in the vertical zone of the wing structure is chosen. The local coordinate system of this element is not coincident with the global one. The python code is able to transform the data of the element from the local to the global coordinate. Once the transformation is done Mul2 code is able to perform the analysis of the element.

The analysis has been performed with 5L9x5L9 elements for the structural mesh (plane x-z) and one element B4 per layer on the y coordinate.

The displacements of the element are validated comparing those found with the global/local model runned by the Mul2 code and those provided by Nastran (Femap). The comparison is shown in the Fig.7.23. As it can be observed the displacements are the same no matters the model, validating the global local CUF model.



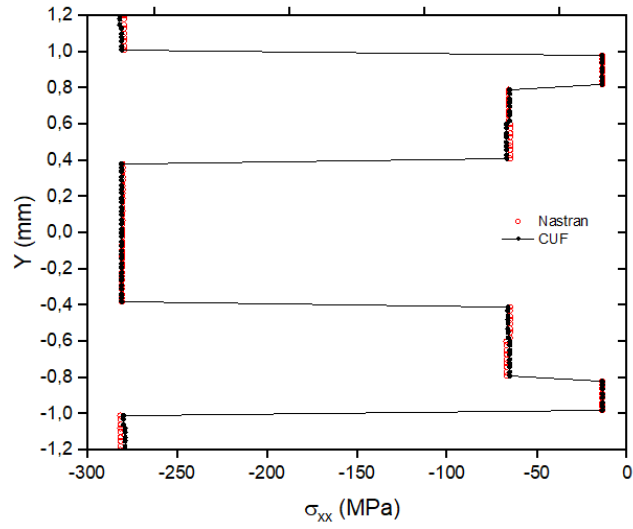
(a) Global displacements - Nastran 2D



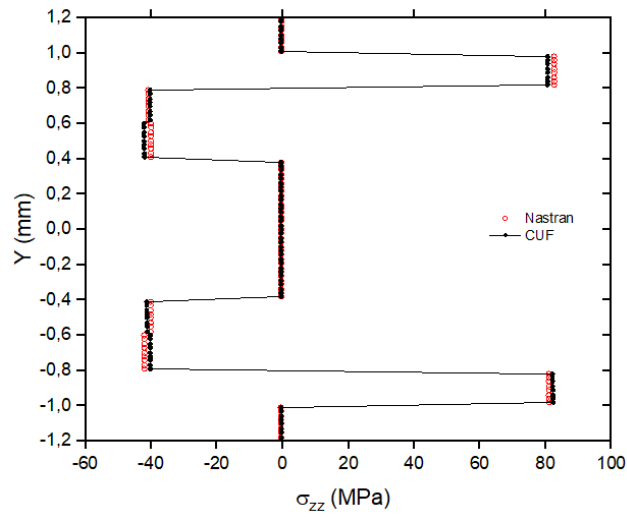
(b) Local displacements - CUF

Figure 7.23: Local and Global displacements of a vertical element

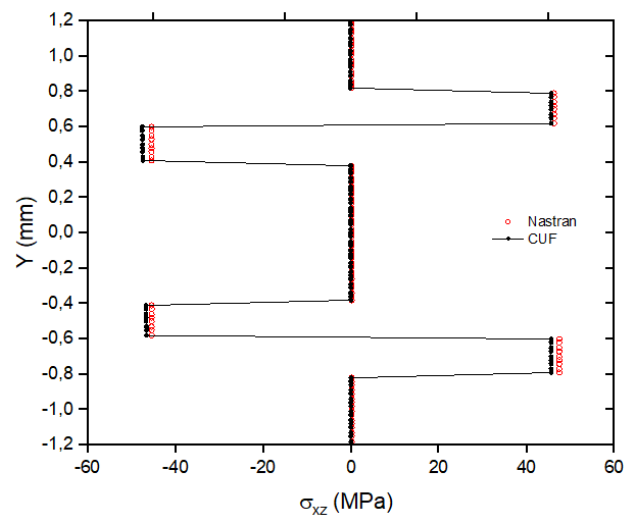
Regarding of the stresses an analysis on the middle point is carried on. The graphs are presented in Fig.7.24. The stresses calculated by Nastran or by te global/local model are pretty similar, validating that the code is performing correctly.



(a) Normal stress - σ_{xx}



(b) Normal stress - σ_{zz}



(c) Shear stress - σ_{xz}

Figure 7.24: Normal and shear stresses on the element middle point

Chapter 8

Conclusions

In this chapter a summary of the work done and the conclusions that can be extracted from this project are presented.

The Carrera Unified Formulation is used to perform local analysis for composite laminates, as the classical beam and plates theories have several limitations in the prediction of high order effects or in-plane deformations. The global local approach consists in the analysis of the global model with a commercial code (normally Nastran) to identify which parts of the model presents complex stress fields fields, where a local analysis is carried out, to perform a local analysis in those parts. Also the free edge effect in composite laminates is better predict by the CUF formulation instead of the calculations made from the commercial code 1D or 2D models.

In the framework of the global local approach a Python interface has been developed. Originally, there was a python interface for the beams models but no for plates. The beam model interface has been improved to be able to work with layers made from different materials and with different orientations. This interface has been validated with a numerical example. Once the beam interface was validated a plate interface was coded to be able to perform in plates the same type of analysis that were done in beams. This plate interface works equal as the beam interface but having the expansion mesh on the z-axis (thickness direction) and the structural mesh in the x-y plane. The results calculated through this plate interface were validated and compared with those calculated with Nastran or with the beam model.

Both beam and plate interface are not able to deal with irregular meshes, elements not

formed by four straight lines parallel two to two (rectangular elements). Moreover the plate and beam interface are only able to work with elements orientated in the y global coordinate in case of the beam and in the x-y plane global coordinates in the case of the plate. This problems are solved with the element wise approach, that permits a local analysis of any element oriented in any direction and without the need to be a rectangular element. This last python interface has also been validated with two different examples

Chapter 9

Appendix

9.1 Python plate interface manual

Nastran

1. Save the bdf file of the Nastran model
2. On the Nastran model select *results to data table* then select the three translations and the three rotations.
3. Once the translations and rotations are selected click done and select the nodes that form the boundary of the local zone to be analysed. In case one or more boundaries are free edge there is no need to select the nodes that conform it.
4. Nastran model will create a table with the translations and rotations of the selected nodes, save this table at the same folder than the bdf file (recommended).

Python interface

1. Run the python code.
2. Select the bdf file of the model that has to be analysed.
3. Select the file with the boundary local zone displacements and rotations. Make sure that Nastran has saved this file with point for decimal separator.
4. Select the case you want to study (Fig.9.1). In case there is no free edge select case 1. On contrary select the case corresponding of your local zone. A and C are the edges with a constant global coordinate y and B and D the edges with constant coordinate x.

```

      § § § D § § §
      §  LOCAL  §
      A          C
      §  REGION  §
      § § § B § § §

Cases:
Case 1 - [A,B,C,D]      Case 6 - [A,B]      Case 11 - [C,D]
Case 2 - [A,D,C]       Case 7 - [A,C]      Case 12 - [A]
Case 3 - [A,B,C]       Case 8 - [A,D]      Case 13 - [B]
Case 4 - [B,C,D]       Case 9 - [B,C]      Case 14 - [C]
Case 5 - [A,B,D]       Case 10 - [B,D]     Case 15 - [D]

Select case number:

```

Figure 9.1: Local zone case selection

5. Decide whether you want to work with Q9 elements or Q16 elements (Fig.9.2).

```

Insert the element type:
Case 0 - Q9
Case 1 - Q16

```

Figure 9.2: Element type selection

6. Decide the type of mesh you want to use between three types as it is shown in Fig.9.3. Equidistant mesh (normal mesh), chebyshev mesh and square chebyshev mesh. This two last meshes are recommended for free edges because they concentrate the nodes on the boundary.

```

Select mesh type:

Case 1 - Equispaced
Case 2 - Chebyshev
Case 3 - Square Chebyshev
Case:

```

Figure 9.3: Mesh type selection

7. The next step is to choose the number of elements (Q9 or Q16 depending on the previous chose) along the plane coordinates x,y, and the number of elements (B4) for each layer that you want to consider (Fig.9.4).

```
Insert the number of elements along x:  
5  
Insert the number of elements along y:  
5  
Insert the number of B4 element per layer:  
2
```

Figure 9.4: Number of elements selection

8. Then the code will open a window with a graph of the structural mesh you have decided (Fig.9.5). Once the window is close you can decide whether you like the structural mesh or do you want to change it (Fig.9.6).

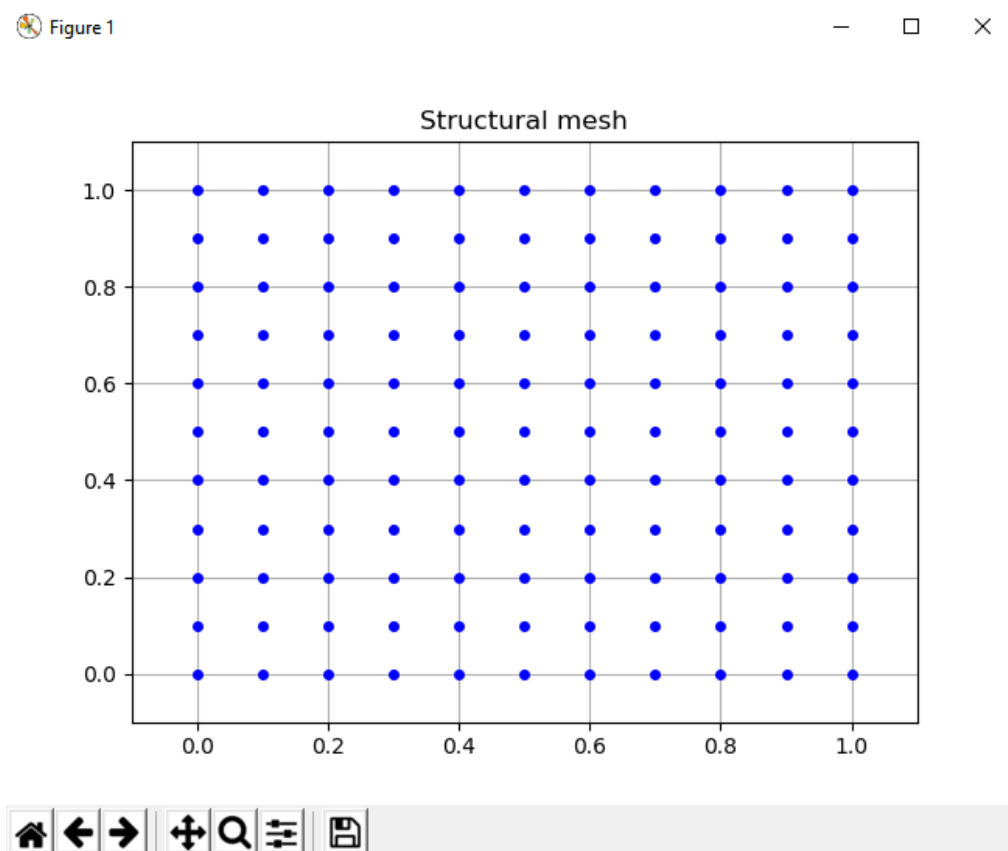


Figure 9.5: Structural mesh

```
Do you like the structural mesh ?  
0 - No  
1 - Yes
```

Figure 9.6: Decision about the satisfaction on the structural mesh

9. Finally the code give you the opion to run automatically the Mul2 code (Fig.9.7).

```
All the input file for the MUL2 code are ready
Press:
- 0 to run an analysis with MUL2 code
- 1 to exit
```

Figure 9.7: Selection whether you like to run Mul2 code or not

9.2 Element wise interface manual

Nastran

1. Save the bdf file of the Nastran model.
2. On the Nastran model select *results to data table* then select the three translations and the three rotations.
3. Once the translations and rotations are selected click done and select the nodes that form the element to be analysed.
4. Nastran model will create a table with the translations and rotations of the selected nodes, save this table at the same folder than the bdf file (recommended).

Python interface

1. Run the python code.
2. Select the bdf file of the model that has to be analysed.
3. Select the file with the nodes displacements and rotations. Make sure that Nastran has saved this file with point for decimal separator.
4. Select if you want to study a case with free edge or not (Fig.9.8).

```
Do you want to consider a case with free edge?:
0 - No
1 - Yes
```

Figure 9.8: Select if a free edge has to be considered

4.1. In case a free edge is selected, the number of free edges to be considered (at the moment only one free edge can be studied) and the nodes that form the free edge have to be indicated as it is displayed in Fig.9.9.

```
Insert the number of free edges that you want consider:
1
Insert the id of the nodes that form the free edge:
First node:
1564
Second node:
1563
```

Figure 9.9: Select the nodes that conform the free edge

5. Decide whether you want to work with Q9 elements or Q16 elements (Fig.9.10).

```
Insert the element type:
Case 0 - Q9
Case 1 - Q16
```

Figure 9.10: Element type selection

6. Decide the type of mesh you want to use between three types as it is shown in Fig.9.11. Equidistant mesh (normal mesh), chebyshev mesh and square chebyshev mesh are available.

```
Select mesh type:
Case 1 - Equispaced
Case 2 - Chebyshev
Case 3 - Square Chebyshev
Case:
```

Figure 9.11: Mesh type selection

7. The next step is to choose the number of elements (Q9 or Q16 depending on the previous chose) along each side of the structural mesh, and the number of elements (B4) for each layer that you want to consider (Fig.9.12).

```
Insert the number of Q9 subdomain along each edge:
10
Insert the number of B4 element per layer:
5
```

Figure 9.12: Number of elements selection

8. Then the code will open a window with a 3D graph of the structural mesh you have decided

(there is an example in Fig.9.13). Once the window is close you can decide wether you like the structural mesh or do you want to change it (Fig.9.14).

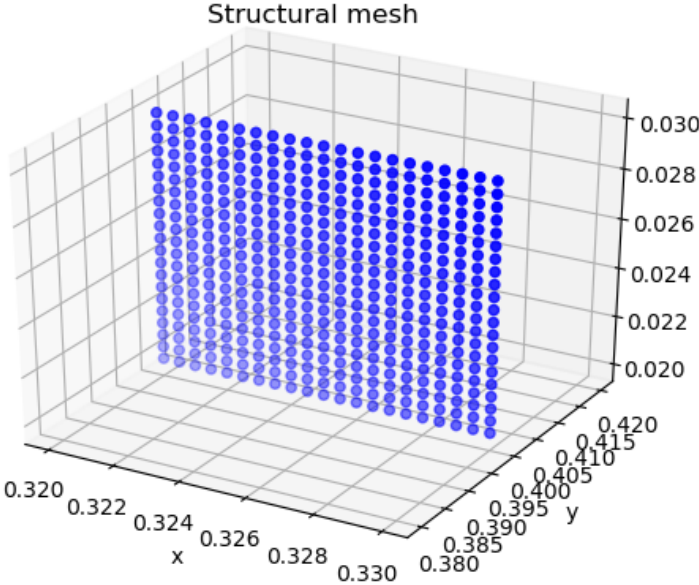


Figure 9.13: Structural mesh

```
Do you like the structural mesh ?  
0 - No  
1 - Yes
```

Figure 9.14: Decision about the satisfaction on the structural mesh

9. Finally the code give you the option to run automatically the Mul2 code (Fig.9.15).

```
All the input file for the MUL2 code are ready  
Press:  
- 0 to run an analysis with MUL2 code  
- 1 to exit
```

Figure 9.15: Selection whether you like to run Mul2 code or not

Bibliography

- [1] M. Petrolo E. Carrera, G. Giunta. *Beam structures: classical and advanced theories*. John Wiley and Sons, 2011.
- [2] A. Pagani E. Carrera, A.G de Miguel. Hierarchical theories of structures based on legendre polynomial expansions with finite element applications. *International Journal of Mechanical Sciences*, 120:286–300, 2017.
- [3] E. Carrera and M. Petrolo. Refined beam elements with only displacement variables and plate/shell capabilities. *Meccanica*, 47(3):537–556, 2012.
- [4] G.A Fiordilino E. Carrera, A. Pagani. Low-fidelity versus high-fidelity finite element models for static, dynamic and aeroelastic analyses of composite wings (lohcv). 2018.
- [5] Alberto García de Miguel. Master thesis: Hierarchical legendre-type 1d cuf-fe’s applied to metallic and composite structures.
- [6] M.Petrolo A. Pagani E. Carrera, A.G de Miguel. Analysis of laminated beams via unified formulation and legendre polynomial expansions. *Composite Structures*, 156:78–92, 2017.
- [7] Mul2 search group : <http://www.mul2.polito.it>.
- [8] G.A Fiordilino A. Pagani E. Carrera, A.G de Miguel. Global/local analysis of free-edge stresses in composite laminates.
- [9] M.Nagaraj A.Pagani M. Montemurro E.Carrera, G.A Fiordilino. Global-local analysis of metallic and composite structures by using various fem models. 2018.
- [10] Alberto Fiordilino. Master thesis: Global-local analysis of aircraft structures by variable kinematics models.

- [11] J Jaap. Wijker. Mechanical vibrations in spacecraft design. *Springer Science and Business*, 2004.
- [12] Lin Liao. A study of inertia relief analysis. *52nd AIAA/ASME/ASCE/AHS/ASC Structures, Structural Dynamics and Materials Conference 19th AIAA/ASME/AHS Adaptive Structures Conference 13t*, 2011.
- [13] E. Carrera and M. Petrolo. Refined beam elements with only displacement variables and plate/shell capabilities. *Meccanica*, 47(3):537–556, 2012.